

1 **Real-time measurements of gas-phase organic acids using SF₆⁻ chemical ionization**
2 **mass spectrometry**

3
4 Theodora Nah,^{1,a} Yi Ji,^{1,2} David J. Tanner,¹ Hongyu Guo,¹ Amy P. Sullivan,³ Nga Lee
5 Ng,^{1,2} Rodney J. Weber¹ and L. Gregory Huey^{1*}

6
7 ¹*School of Earth and Atmospheric Sciences, Georgia Institute of Technology, Atlanta, GA, USA*

8 ²*School of Chemical and Biomolecular Engineering, Georgia Institute of Technology, Atlanta, GA, USA*

9 ³*Department of Atmospheric Science, Colorado State University, Fort Collins, CO, USA*

10 ^a*Now at School of Energy and Environment, City University of Hong Kong, Kowloon, Hong Kong, China*

11 ** To whom correspondence should be addressed: greg.huey@eas.gatech.edu*
12

13 **Abstract**

14 The sources and atmospheric chemistry of gas-phase organic acids are currently poorly
15 understood due in part to the limited range of measurement techniques available. In this
16 work, we evaluated the use of SF₆⁻ as a sensitive and selective chemical ionization reagent
17 ion for real-time measurements of gas-phase organic acids. Field measurements are made
18 using a chemical ionization mass spectrometer (CIMS) at a rural site in Yorkville, Georgia
19 from September to October 2016 to investigate the capability of this measurement
20 technique. Our measurements demonstrate that SF₆⁻ can be used to measure a range of
21 organic acids in the atmosphere. 1-hour averaged ambient concentrations of organic acids
22 ranged from a few parts per trillion by volume (ppt) to several parts per billion by volume
23 (ppb). All the organic acids displayed similar strong diurnal behaviors, reaching maximum
24 concentrations between 5 and 7 pm local time. The organic acid concentrations are
25 dependent on ambient temperature, with higher organic acid concentrations being
26 measured during warmer periods.

27 **Introduction**

28 Organic acids are ubiquitous and important species in the troposphere. They are
29 major contributors of free acidity in precipitation (Galloway et al., 1982; Keene et al., 1983;
30 Keene and Galloway, 1984), and can also affect the formation of secondary organic
31 aerosols (SOA) (Zhang et al., 2004; Carlton et al., 2006; Sorooshian et al., 2010; Yatavelli
32 et al., 2015). As end products of oxidation, organic acids can also serve as useful tracers of
33 air mass history (Sorooshian et al., 2007; Sorooshian et al., 2010). Organic acids are found
34 in urban, rural and remote marine environments in the gas, aqueous and particle phases.

35 While organic acids are emitted directly from biogenic sources (e.g., microbial activity,
36 vegetation and soil) and anthropogenic activities (e.g., fossil fuel combustion, vehicular
37 emissions and biomass burning) (Kawamura et al., 1985; Talbot et al., 1988; Chebbi and
38 Carlier, 1996; Talbot et al., 1999; Seco et al., 2007; Veres et al., 2010; Paulot et al., 2011;
39 Veres et al., 2011; Millet et al., 2015), they can also be formed from photooxidation of
40 non-methane volatile organic compounds and aqueous-phase photochemistry of semi-
41 volatile organic compounds (Chebbi and Carlier, 1996; Hansen et al., 2003; Orzechowska
42 and Paulson, 2005; Carlton et al., 2006; Sorooshian et al., 2007; Ervens et al., 2008; Paulot
43 et al., 2011; Millet et al., 2015). The chemical aging of organic aerosols has also been
44 proposed as a major source of organic acids (Molina et al., 2004; Vlasenko et al., 2008;
45 Paulot et al., 2011). The relative importance of primary and secondary sources of organic
46 acids are currently poorly constrained though their emissions likely depend on the
47 magnitude of biogenic and anthropogenic activities and the meteorological conditions. Wet
48 and dry deposition are the primary sinks of organic acids in the atmosphere (Chebbi and
49 Carlier, 1996).

50 Formic and acetic acids are the dominant gas-phase monocarboxylic acids in the
51 troposphere (Chebbi and Carlier, 1996). Due to their high vapor pressures, the gas-phase
52 concentrations of formic and acetic acids are usually 1 to 2 orders of magnitudes higher
53 than their particle-phase concentrations. Some field studies report strong correlations
54 between formic and acetic acids, suggesting that these two organic acids have similar
55 sources (Nolte et al., 1997; Souza and Carvalho, 2001; Paulot et al., 2011). A recent
56 modeling study suggested that the dominant sources of formic acid in the southeastern U.S.
57 are primarily biogenic in nature (Millet et al., 2015). These sources include direct emissions
58 from vegetation and soil and photochemical production from biogenic volatile organic
59 compounds (BVOCs). Currently, atmospheric formic and acetic acid concentrations are
60 higher than those predicted by models, indicating that present model estimates of source
61 and sink magnitudes are incorrect (Paulot et al., 2011; Millet et al., 2015). In the case of
62 formic acid, deposition and secondary photochemical production via mechanisms such as
63 photooxidation of isoprene and reaction of stabilized criegee intermediates need to be
64 better constrained in models. Given that formic and acetic acids are major trace gases in
65 the atmosphere, there is a need to resolve the discrepancy between measurements and

66 model predictions to close the atmospheric reactive carbon budget and improve our overall
67 understanding of VOC chemistry in the atmosphere.

68 Currently, research on gas-phase organic acids has focused primarily on formic and
69 acetic acids (Andreae et al., 1988; Talbot et al., 1988; Grosjean, 1991; Hartmann et al.,
70 1991; Talbot et al., 1995; Talbot et al., 1999). This is due, in part, to the analytical
71 difficulties in measuring gas-phase $> C_2$ organic acids and oxidized organic acids (i.e.,
72 containing more than 2 oxygen atoms) in real time. These organic acids have low vapor
73 pressures and are generally present in low concentrations in the gas phase. For example,
74 dicarboxylic acids typically have vapor pressures that are 2 to 4 orders of magnitude lower
75 than their analogous monocarboxylic acids (Chebbi and Carlier, 1996), and are present
76 mainly in the particle and aqueous phases. Rapid and accurate measurements of gas-phase
77 $> C_2$ organic acids and oxidized organic acids are necessary for constraining the regional
78 and global SOA budget since these acids can partition readily between the gas and particle
79 and aqueous phases and subsequently affect SOA formation (Zhang et al., 2004; Carlton
80 et al., 2006; Ervens et al., 2008; Sorooshian et al., 2010; Yatavelli et al., 2015).

81 Chemical ionization mass spectrometry (CIMS) is commonly used to selectively
82 measure atmospheric trace gases in real-time with high sensitivity. CIMS measurements
83 rely on reactions between reagent ions and compounds of interest present in the sampled
84 air to produce analyte ions that are detected by a mass spectrometer. The subset of
85 molecular species detected is determined by the reagent ion employed since the specificity
86 of the ionization process is governed by the ion-molecule reaction mechanism. CIMS is a
87 popular tool for atmospheric measurements since it is versatile and has high time resolution
88 and sensitivity. It is also often a soft ionization technique with minimal ion fragmentation,
89 thus preserving the parent molecule's elemental composition and allowing for molecular
90 speciation. Recent developments in chemical ionization methods and sources have greatly
91 improved our ability to measure atmospheric acidic species. Some of the CIMS reagent
92 ions that have been used to measure atmospheric organic acids include acetate ($CH_3CO_2^-$),
93 iodide (I^-) and CF_3O^- anions (Crouse et al., 2006; Veres et al., 2008; Lee et al., 2014;
94 Brophy and Farmer, 2015; Nguyen et al., 2015). However, each of these CIMS reagent
95 ions has its drawbacks, which are generally related to their selectivity and sensitivity

96 towards different atmospheric species. For example, acetic acid is difficult to measure with
97 CH_3CO_2^- as the CIMS reagent ion due to interferences from the reagent ion chemistry that
98 complicates the desired ion-molecule reactions. In addition, while many organic acids can
99 be detected using I^- as a reagent ion, its sensitivity to different acids can vary by orders of
100 magnitude (Lee et al., 2014).

101 The sulfur hexafluoride (SF_6^-) anion has been used as a CIMS reagent ion to
102 measure atmospheric inorganic species such as sulfur dioxide (SO_2), nitric acid (HNO_3)
103 and peroxyxynitric acid (HO_2NO_2) (Slusher et al., 2001; Slusher et al., 2002; Huey et al.,
104 2004; Kim et al., 2007). SF_6^- commonly reacts with most acidic gases at the collision rate
105 by either proton or fluoride transfer reactions (Huey et al., 1995). The SF_6^- ion chemistry
106 is selective to acidic species, which can simplify the mass spectral analysis of organic acids.
107 However, SF_6^- is reactive to both ozone (O_3) and water vapor, which can lead to interfering
108 reactions that limit its applicability to many species in certain environments (Huey et al.,
109 2004). For these reasons, this work is focused on assessing the ability of SF_6^- to measure a
110 series of organic acids in ambient air. The major advantage that SF_6^- has over I^- and
111 CH_3CO_2^- is that it allows for the detection of acetic acid and SO_2 . CF_3O^- has a similar
112 chemistry to SF_6^- but it also has issues due to hydrolysis and the ion precursor is not
113 commercially available. We present ambient measurements of gas-phase organic acids
114 conducted in a mixed forest-agricultural area in Georgia in early fall of 2016 to evaluate
115 the performance of a SF_6^- CIMS technique. Gas-phase organic acid measurements are
116 compared to gas-phase water-soluble organic carbon (WSOC_g) measurements performed
117 during the field study to estimate the fraction of WSOC_g that is comprised of organic acids
118 at this rural site. Laboratory experiments are conducted to measure the sensitivity of SF_6^-
119 with a series of organic acids of atmospheric relevance.

120 **2. Methods**

121 **2.1. Field site**

122 Real-time ambient measurements of gas-phase organic acids were obtained using a
123 chemical ionization mass spectrometer from 3 Sept to 12 Oct 2016 at the SouthEastern
124 Aerosol Research and Characterization (SEARCH) site located in Yorkville, Georgia. A

125 detailed description of the field site has been provided by Hansen et al. (2003). Briefly, the
126 Yorkville field site (33.931 N, 85.046 W) was located ~55 km northwest of Atlanta (the
127 closest urban center), and was on a broad ridge in a large pasture where there were
128 occasionally grazing cattle. The field site was surrounded by forest and agricultural land.
129 There were no major roads near the field site and nearby traffic emissions were negligible.
130 The closest power plant was Plant Bowen, which was located ~25 km north of the field
131 site. The sampling period was characterized by moderate temperatures (24.0 °C average,
132 32.6 °C max, 9.5 °C min) and high relative humidities (68.9 % RH average, 100 % RH
133 max, 21.6 % RH min). The study-averaged diurnal trends of relative humidity, temperature
134 and solar radiance are shown in Fig. S1. Data reported are displayed in EDT. Volumetric
135 gas concentrations reported are at ambient temperature and relative humidity.

136 **2.2. SF₆-CIMS**

137 **2.2.1. CIMS instrument and air sampling inlet**

138 The CIMS instrument was housed in a temperature-controlled trailer during the
139 field study. The inlet configuration and CIMS instrument used in this study is shown in
140 Fig. 1. Since HNO₃ and organic acids may condense on surfaces, an inlet configuration
141 with a minimal wall interaction was used. This inlet configuration was previously described
142 by Huey et al. (2004) and Nowak et al. (2006); hence, only a brief description will be
143 provided here. The inlet was a 7.6 cm ID aluminum pipe that extended ~40 cm into the
144 ambient air through a hole in the trailer's wall. This positioned the inlet ~2 m above the
145 ground. A donut-shaped ring was attached to the ambient sampling port of the pipe to
146 reduce the influence of crosswinds on the pipe's flow dynamics. This ring was wrapped
147 with a fine wire mesh to prevent insects from being drawn through the pipe. A flow of
148 ~2800 L min⁻¹ was maintained in the pipe using a regenerative blower (AMETEK
149 Windjammer 116637-03). Part of this flow (7 L min⁻¹) was sampled through a custom-
150 made three-way PFA Teflon valve, which connected the pipe's center to the CIMS
151 sampling orifice. The valve was maintained at a temperature of 40 °C in an insulated
152 aluminum oven and could be switched automatically between ambient and background
153 modes. In ambient mode, ambient air was passed through a 25 cm long, 0.65 cm ID Teflon

154 tube into the CIMS. In background mode, ambient air was first drawn through an activated
155 charcoal scrubber before being delivered into the CIMS. A small flow of ambient air (~ 0.05
156 L min^{-1}) was continuously passed through the scrubber to keep it at equilibrium with
157 ambient humidity levels. Most of the sampled air flow (6.7 L min^{-1}) was exhausted using
158 a small diaphragm pump. The rest of the sampled air flow (0.3 L min^{-1}) was introduced
159 into the CIMS instrument through an automatic variable orifice, which was used to
160 maintain a constant sample air mass flow.

161 The CIMS instrument was comprised of a series of differentially pumped regions:
162 a flow tube, a collisional dissociation chamber, an octopole ion guide, a quadrupole mass
163 filter and an ion detector. These sections were evacuated by a scroll pump (Edward nXDS
164 20i), a drag pump (Adixen MDP 5011) and two turbo pumps (Varian Turbo-V301),
165 respectively. Ambient air was drawn continuously into the flow tube. A flow of 3.7
166 standard liter per minute (slpm) of N_2 containing a few ppm of SF_6 (Scott-Marrin Inc.) was
167 passed through a ^{210}Po ion source into the flow tube. SF_6^- anions, which were produced via
168 associative electron attachment in the ^{210}Po ion source, reacted with the sampled ambient
169 air in the flow tube to generate analyte ions. Arnold and Viggiano (2001) showed that the
170 formation of $\text{F}^{\cdot}(\text{HF})_n$ cluster ions from the reaction of SF_6^- and water vapor is enhanced at
171 high flow tube pressures. Since these $\text{F}^{\cdot}(\text{HF})_n$ cluster ions could interfere with mass
172 spectral analysis, the flow tube was maintained at a low pressure ($\sim 13 \text{ mbar}$, 0.5 %
173 uncertainty) in this study to reduce both the water vapor concentration and reaction time in
174 the flow tube, thus minimizing interferences from SF_6^- reaction with water vapor. The
175 analyte ions exited the flow tube and were accelerated through the collisional dissociation
176 chamber (CDC), which was maintained at $\sim 0.8 \text{ mbar}$ (10 % uncertainty). The molecular
177 collisions in the CDC served to dissociate weakly bound cluster ions into their core ions to
178 simplify mass spectral analysis. Flow tube and CDC pressures were controlled by the
179 automatic variable orifice. For this study, the CDC was operated at a relatively high electric
180 field ($\sim 113 \text{ V cm}^{-1}$) to efficiently dissociate cluster ions. The resulting ions were then
181 passed into the octopole ion guide (maintained at $\sim 6 \times 10^{-3} \text{ mbar}$), which collimated the
182 ions and transferred them into the quadrupole mass spectrometer (maintained at $\sim 10^{-5}$
183 mbar) for mass selection and detection. It should also be noted that we always used gloves
184 when working on the CIMS during this study to limit contamination of lactic acid

185 emissions from human skin. In addition, we kept people away from the front of the SF₆-
186 CIMS sampling inlet to minimize lactic acid interferences as well.

187 Ions monitored during the field study included mass-to-charge ratio (m/z) 45, 59,
188 65, 73, 75, 79, 82, 87, 89, 101, 102, 103, 108, 117, 131 and 148. The assignment of these
189 ions will be discussed in section 3. The dwell time for each m/z ion was set to 0.5 s and
190 measurements of these ions were obtained every ~13 s, which resulted in a ~4 % (= 0.5/13
191 x 100 %) duty cycle for each ion monitored. The data presented in this paper was averaged
192 to 1-hour intervals unless stated otherwise.

193 **2.2.2. Background and calibration measurements during field study**

194 Background measurements were performed every 25 min during the field study.
195 During each background measurement, the sampled air flow was passed through an
196 activated charcoal scrubber prior to delivery into the CIMS. The scrubber removed > 99 %
197 of the targeted species in ambient air. Calibration measurements were performed every 5 h
198 during the field study through standard additions of ³⁴SO₂ and either formic or acetic acid
199 to the sampled air flow. Each background and calibration measurement period lasted ~4
200 and ~3.5 min, respectively, which not only gave the scrubber (during background
201 measurements) and flow tube ample time to equilibrate when the three-way PFA Teflon
202 valve was switched between ambient and background modes, but also allowed us to obtain
203 good averaging statistics during background and calibration measurements. A 1.12 ppm
204 ³⁴SO₂ gas standard was used as the source of the sulfur standard addition. 1.85 ppb of ³⁴SO₂
205 was added to sampled air flow during calibration measurements. The formic and acetic
206 acid calibration sources were permeation tubes (VICI Metronics) with emission rates of 91
207 and 110 ng min⁻¹, respectively. The emission rates were measured by scrubbing the output
208 of the permeation tube in deionized water via a gas impinger immersed in water, which
209 was then analyzed for formate and acetate using ion chromatography (Thermo Fisher
210 Scientific). Eight samples of each acid were analyzed over the course of the field study and
211 the standard deviations of the permeation rates were ≤ 6 %. 6.75 ppb of formic acid and
212 5.87 ppb of acetic acid was added to sampled air flow during calibration measurements.
213 The CIMS instrument sensitivity measured by the F₂³⁴SO₂⁻ ion signal (m/z 104) was
214 similarly applied to all the other measured species (except for formic and acetic acids)

215 using relative sensitivities determined in laboratory studies. The $F_2^{34}SO_2^-$ calibrant ion
216 signals were also used to calibrate ambient $F_2^{32}SO_2^-$ ion signals and determine ambient SO_2
217 concentrations as discussed in section 3.2.5.

218 **2.2.3. Laboratory calibration**

219 To estimate the levels of sensitivities for a series of acids of atmospheric relevance,
220 HNO_3 , oxalic, butyric, glycolic, propionic and valeric acid standard addition calibrations
221 were performed in post-field laboratory work. Many of these acids have previously been
222 measured in rural and urban environments (Kawamura et al., 1985; Veres et al., 2011;
223 Brophy and Farmer, 2015). The response of the CIMS acid signals were measured relative
224 to the sensitivity of $^{34}SO_2$ in these calibration measurements. The HNO_3 calibration source
225 was a permeation tube (KIN-TEK) with a permeation rate of 39 ng min^{-1} , which was
226 measured using UV optical absorption (Neuman et al., 2003). Solid or liquid samples of
227 oxalic (Sigma Aldrich, $\geq 99 \%$), butyric (Sigma Aldrich, $\geq 99 \%$), glycolic (Sigma Aldrich,
228 99%), propionic (Sigma Aldrich, $\geq 99.5 \%$) and valeric (Sigma Aldrich, $\geq 99 \%$) acids
229 were used in calibration measurements. The acid sample was placed in a glass impinger,
230 which was immersed in an ice bath to provide a constant vapor pressure. A flow of 6 to 10
231 mL min^{-1} of N_2 was passed over the organic acid in the glass impinger. This organic acid
232 air stream was then diluted with varying flows of N_2 (1 to 5 L min^{-1}) to achieve different
233 mixing ratios of the organic acid. Mixing ratios were calculated from either the acid's
234 emission rate from the impinger or the acid's vapor pressure. The emission rate of gas-
235 phase oxalic acid from the impinger was measured by scrubbing the output in deionized
236 water using the same method for calibrating the formic and acetic acid permeation tubes,
237 followed by ion chromatography analysis for oxalate. Three samples were analyzed and
238 the emission rate was determined to be 14 ng min^{-1} with a standard deviation of $< 5 \%$. The
239 vapor pressures of butyric and propionic acids at $0 \text{ }^\circ\text{C}$ were measured using a capacitance
240 manometer (MKS Instruments). The vapor pressures of glycolic and valeric acids at $0 \text{ }^\circ\text{C}$
241 were estimated using their literature vapor pressures at $25 \text{ }^\circ\text{C}$ and enthalpies of vaporization
242 (Daubert and Danner, 1989; Lide, 1995; Acree and Chickos, 2010).

243 Attempts to generate a calibration plot for pyruvic acid using its liquid sample
244 (Sigma Aldrich, 98%) and the setup described above were unsuccessful as this acid was

245 found to interact very strongly with surfaces. Glyoxylic acid calibrations were not
246 performed due to the presence of impurities in the glyoxylic acid monohydrate solution
247 used (Sigma Aldrich, 98 %), which resulted in the appearance of ions not attributed to
248 glyoxylic acid. We attempted to generate calibration plots for malonic (Sigma Aldrich, \geq
249 99.5 %), succinic (Sigma Aldrich, 99 %) and glutaric (Sigma Aldrich, 99 %) acids by
250 passing N₂ over their solid samples at room temperature. However, it was not possible to
251 generate large enough gas phase concentrations for calibration since these organic acids
252 have very low vapor pressures. The vapor pressures of malonic, succinic and glutaric acids
253 are 5.73×10^{-4} , 1.13×10^{-4} and 4.21×10^{-4} kPa at 298 K, respectively (Booth et al., 2010),
254 which are at least 2 orders of magnitude lower than the organic acids that we calibrated.
255 Although heating up the malonic, succinic and glutaric acid samples will likely generate
256 sufficient vapors for calibration, this method of generating calibrant gases will lead to large
257 measurement uncertainties due to vapors condensing out and adhering onto surfaces at
258 room temperature prior to introduction into the CIMS.

259 **2.2.4. Detection limits and measurement uncertainties**

260 The detection limits of the organic acids were estimated as 3 times the standard
261 deviation values (3σ) of the ion signals measured during background mode. Although each
262 background measurement period lasted ~ 4 min, ion signals of the different organic acids
263 took up to 1.5 min to stabilize during the switch between ambient, calibration and
264 background measurements during the field study. Thus, ion signals measured during the
265 first 1.5 min were not included in the calculation of the average and standard deviation of
266 ion signals measured during background mode. Table 1 summarizes the average detection
267 limits of calibrated organic acids for 2.5 min averaging periods which corresponds to the
268 length of a background measurement with a 4 % duty cycle for each m/z. The mean
269 difference between successive background measurements ranged from 1 to 40 ppt for the
270 different organic acids. Future work will focus on reducing the instrument background, and
271 therefore improving the detection limits of these organic acids.

272 The uncertainties (1σ) in our ambient measurements of formic, acetic and oxalic
273 acid concentrations originated from CIMS and ion chromatography calibration
274 measurements. The ion chromatography measurement uncertainty was estimated to be 10

275 % . For formic and acetic acids, which were calibrated during the field study using
276 permeation tubes, their CIMS measurement uncertainties were estimated to be 6 and 7 %,
277 respectively, based on one standard deviation of the acids' calibrant ion signals. For oxalic
278 acid, which was calibrated in post-field laboratory work, the CIMS measurement
279 uncertainty was estimated to be 9 % based on one standard deviation of the $^{34}\text{SO}_2$
280 sensitivity (3 %), the acid's calibrant ion signals (7 %) and linear fit of the calibration curve
281 (5 %). Hence, the uncertainties in our ambient measurements of formic, acetic and oxalic
282 acid concentrations were estimated to be 12, 12 and 14 %, respectively.

283 For nitric acid, which was calibrated in post-field laboratory work using a
284 permeation tube and UV optical absorption, the uncertainty in its ambient concentrations
285 was estimated to be 13 % based on uncertainties in UV absorption measurements (10 %)
286 and one standard deviation of the acid's UV absorption signals (3 %), $^{34}\text{SO}_2$ sensitivity (3
287 %) and acid's calibrant ion signals (8 %). For propionic acid, which was calibrated in post-
288 field laboratory work using vapor pressures measured by a capacitance manometer, the
289 uncertainty in its ambient concentrations was estimated to be 14 % based on the vapor
290 pressure measurement uncertainty (10 %) and one standard deviation of the $^{34}\text{SO}_2$
291 sensitivity (3 %), the acid's calibrant ion signals (8 %) and linear fits of the acid's
292 calibration curves (3 %). Ambient concentrations and the corresponding uncertainties of
293 glycolic, valeric and butyric acids were not quantified.

294 **2.3. WSOC_g measurements**

295 WSOC_g was measured with a MIST chamber coupled to a total organic carbon
296 (TOC) analyzer (Sievers 900 series, GE Analytical Instruments). Ambient air first passed
297 through a Teflon filter (45 mm diameter, 2.0 μm pore size, Pall Life Sciences) to remove
298 particles in the air stream. This filter was changed every 3 to 4 days. The particle-free air
299 was then pulled into a glass Mist Chamber filled with ultrapure deionized water at a flow
300 rate of 20 L min⁻¹. The MIST chamber scrubbed soluble gases with Henry's law constants
301 greater than 10³ M atm⁻¹ into deionized water (Spaulding et al., 2002). The resulting liquid
302 samples from the MIST chamber were analyzed by the TOC analyzer. The TOC analyzer
303 converted the organic carbon in the liquid samples to carbon dioxide using UV light and
304 chemical oxidation. The carbon dioxide formed was then measured by conductivity. The

305 amount of organic carbon in the liquid samples is proportional to the measured increase in
306 conductivity of the dissolved carbon dioxide. Each WSOC_g measurement lasted 4 min.
307 Background WSOC_g measurements were performed for 45 min every 12 h by stopping the
308 sample air flow and rinsing the sampling lines with deionized water. The TOC analyzer
309 was calibrated using different concentrations of sucrose (as specified by the instrument
310 manual) before and after the field study. The limit of detection was 0.4 μgC m⁻³. The
311 measurement uncertainty was estimated to be 10 % based on uncertainties in the sample
312 air flow, liquid flow and TOC analyzer uncertainty. The MIST chamber and upstream
313 particle filter were located in an air-conditioned building so were generally below ambient
314 temperature. Hence, evaporation of collected particles (which will lead to positive artifacts
315 in WSOC_g measurements) are not expected to be significant.

316 **2.4. Supporting gas measurements**

317 Supporting gas measurements were provided by a suite of instruments operated by
318 the SEARCH network. A non-dispersive infrared spectrometer (Thermo Fisher Scientific)
319 provided hourly CO measurements. A UV absorption analyzer (Thermo Fisher Scientific)
320 provided hourly O₃ measurements. A gas chromatography-flame ionization detector (GC-
321 FID, Agilent Technologies) provided hourly VOC measurements.

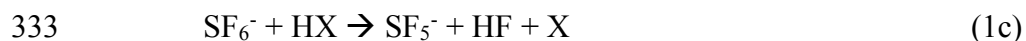
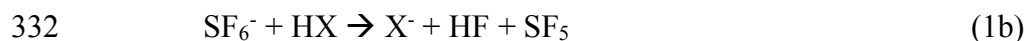
322 **3. Results and discussion**

323 **3.1. General SF₆⁻ CIMS field performance**

324 **3.1.1. SF₆⁻ ion chemistry with organic acids**

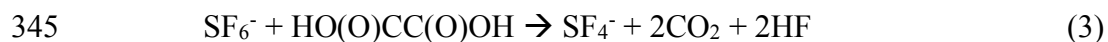
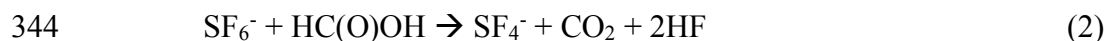
325 CIMS measurements of atmospheric constituents use ion-molecule reactions to
326 selectively ionize compounds of interest in the complex matrix of ambient air and produce
327 characteristic ions. The reactions of SF₆⁻ with the organic acids (HX) proceed through
328 reactions 1a to 1c, and gave similar products to those reported previously for SF₆⁻ reactions
329 with inorganic acids (Huey et al., 1995): SF₅⁻, X⁻ and X⁻•HF where X⁻ is the conjugate base
330 of the organic acid (reactions 1a-c).





334 The effective branching ratios of the SF_5^- , X^- and $\text{X}^- \cdot \text{HF}$ product ions can be impacted by
335 the field strength of the CDC. The SF_5^- ion (m/z 127, reaction 1c) is a common reaction
336 product of the reactions of SF_6^- with many species and is probably thermodynamically
337 driven by the formation of HF (Huey et al., 1995). Unfortunately, the production of SF_5^-
338 does not allow for the selective detection of any atmospheric species. In addition, the larger
339 the branching ratio of the SF_5^- channel, the lower the CIMS sensitivity is to an individual
340 acid since the effective rate constants for the X^- and $\text{X}^- \cdot \text{HF}$ channels are lower.

341 The reaction of SF_6^- with formic acid and oxalic acid also produced SF_4^- ions (m/z
342 108). These reactions are probably thermodynamically driven by the formation of CO_2 and
343 HF:



346 We used the X^- and/or $\text{X}^- \cdot \text{HF}$ ions to determine ambient organic acid concentrations
347 since these ions are characteristic of the individual acids. For all the organic acids, the X^-
348 $\cdot \text{HF}$ ion signal is substantially lower than that of the X^- ion for the conditions in this study.
349 However, this is probably largely due to the relatively high collision energy used in the
350 CDC, which led to efficient dissociation of the fluoride adducts to form X^- ions.
351 Consequently, only the proton transfer channel (1b) is used to quantify most of the organic
352 acids in the field study. The exceptions are formic and acetic acid as discussed in section
353 3.2.1 and 3.2.2

354 Table 1 shows a summary of the sensitivities of X^- and $\text{X}^- \cdot \text{HF}$ ions of some common
355 atmospheric organic acids. The average sensitivities of the HCOO^- (m/z 45) and HCOO^-
356 $\cdot \text{HF}$ (m/z 65) ions of formic acid were 1.29 ± 0.22 and 0.29 ± 0.05 Hz ppt⁻¹, respectively,
357 while the average sensitivities of the CH_3COO^- (m/z 59) and $\text{CH}_3\text{COO}^- \cdot \text{HF}$ (m/z 79) ions
358 of acetic acid were 1.46 ± 0.29 and 0.30 ± 0.06 Hz ppt⁻¹, respectively. A weak ²¹⁰Po ion
359 source (< 1 mCi) was used by SF_6^- -CIMS instrument during the field study, hence these

360 sensitivities will be substantially higher if a stronger radioactive source is used. Post-field
361 laboratory work suggest that the sensitivities may increase by as much as a factor of 5 for
362 a new commercial 20 mCi ^{210}Po ion source. Nevertheless, these sensitivities are compared
363 to formic and acetic acid sensitivities measured by a high-resolution time-of-flight
364 chemical ionization mass spectrometer (Aerodyne Research Inc.) that utilized I^- reagent
365 ions during the field study. Although the formic acid sensitivity measured by I^- -CIMS (1.33
366 ± 0.28 Hz ppt $^{-1}$) was comparable to that measured by SF_6^- -CIMS, the acetic acid sensitivity
367 measured by I^- -CIMS (< 0.1 Hz ppt $^{-1}$) was substantially lower than that measured by SF_6^- -
368 CIMS. Previous studies have similarly reported low acetic acid sensitivity measured by I^- -
369 CIMS (Aljawhary et al., 2013; Lee et al., 2014).

370 **3.1.2. Characterization of interferences**

371 SF_6^- is very sensitive to many trace atmospheric species but its reactions with water
372 vapor and O_3 when sampling ambient air can lead to issues both with selectivity and
373 stability. For example, SF_6^- reacts nonlinearly with water vapor to form a series of $\text{F}^-\cdot(\text{HF})_n$
374 cluster ions (Huey et al., 1995; Arnold and Viggiano, 2001). SF_6^- also reacts efficiently
375 with O_3 to form O_3^- , which is rapidly converted to CO_3^- in ambient air (Slusher et al., 2001).
376 These reactions can deplete SF_6^- as well as form a variety of potentially interfering ions
377 from secondary reactions (e.g., $\text{F}^-\cdot(\text{HF})_n$ and CO_3^- ions) that depend on more abundant
378 atmospheric species. For these reasons, efforts were made to minimize interferences by
379 limiting reaction times and the flow sampled into the CIMS. This was accomplished by
380 sampling only 0.3 L min^{-1} of air through the variable orifice into the flow tube and
381 maintaining the flow tube at a low pressure (~ 13 mbar). The 0.3 L min^{-1} sampled air flow
382 is diluted by 3.7 slpm of N_2/SF_6 flow in the flow tube. The ratio of the sampled air flow to
383 the N_2/SF_6 flow introduced into the flow tube is approximately 1:13. While the high N_2/SF_6
384 flow (3.7 slpm) passed through the radioactive source into the flow tube increased the SF_6^-
385 reagent ion signal, the high dilution of the sampled air flow in the flow tube reduced the
386 CIMS instrument sensitivity by decreasing the number density of the analytes.

387 Figure 2 shows a mass spectrum of ambient air. Interference peaks at m/z 39 ($\text{F}^-\cdot(\text{HF})$
388 and CO_3^- , respectively) can be attributed to the presence of water and O_3 ,
389 respectively. The reagent ion $^{32}\text{SF}_6^-$ is present at m/z 146. The $^{32}\text{SF}_6^-$ reagent ion signal was

390 saturated, and this caused the sharp drop in the m/z 146 signal as shown in Fig. 2. Since
391 the $^{32}\text{SF}_6^-$ reagent ion signal was saturated for the entire field study, we monitored the ion
392 signal of its isotope $^{34}\text{SF}_6^-$ to determine if the reaction of SF_6^- with ambient water vapor
393 (5.92×10^{-6} to 2.19×10^{-5} g cm^{-3}) and O_3 (2.1 to 82.4 ppb) depleted SF_6^- reagent ions.
394 Figure S2a shows the time series of the $^{34}\text{SF}_6^-$ ion signal and ambient water vapor
395 concentration for the entire field study. Despite fluctuations in ambient water vapor and O_3
396 concentrations, the $^{34}\text{SF}_6^-$ ion signal was relatively constant for the entire field study with
397 a standard deviation of $< 3\%$. This indicates that the reaction of SF_6^- with ambient water
398 vapor and O_3 did not significantly deplete the $^{32}\text{SF}_6^-$ reagent ions during the field study.

399 The $\text{F}_2^{34}\text{SO}_2^-$ ion signal was used to monitor the CIMS SO_2 sensitivity during the
400 field study. Figure S2b shows the time series of the $\text{F}_2^{34}\text{SO}_2^-/^{34}\text{SF}_6^-$ ion signal ratio obtained
401 in calibration measurements. There is a $\sim 50\%$ increase in the $\text{F}_2^{34}\text{SO}_2^-/^{34}\text{SF}_6^-$ ion signal
402 ratio on 28 Sept 2016, indicating an increase in the CIMS instrument sensitivity. The
403 increase in CIMS instrument sensitivity is due to the decrease in ambient water vapor
404 concentrations on 28 Sept 2016 (Fig. S2a). Previous laboratory and field studies showed
405 that this was due to the hydrolysis of $\text{F}_2^{34}\text{SO}_2^-$, which led to the loss of this ion and
406 diminished sensitivity at higher levels of ambient water vapor (Arnold and Viggiano, 2001;
407 Slusher et al., 2001). However, the SO_2 sensitivity at $\text{F}_2^{34}\text{SO}_2^-$ only varied within a factor
408 of two for the entire field study with a clear relationship to water vapor (Fig. S2c). The SO_2
409 sensitivity did not show any obvious dependence on ambient O_3 concentrations (Fig. S2d).

410 The formic (HCOO^- at m/z 45 and $\text{HCOO}\cdot\text{HF}$ at m/z 65) and acetic (CH_3COO^-
411 $\cdot\text{HF}$ at m/z 79) acid ions did not show any obvious dependence on ambient water vapor
412 and O_3 concentrations during calibration measurements (Fig. S3). Therefore, we do not
413 expect the sensitivities of the X^- and $\text{X}\cdot\text{HF}$ ions of the studied organic acids to depend on
414 ambient water vapor and O_3 concentrations. We accounted for water vapor dependence of
415 the $\text{F}_2^{34}\text{SO}_2^-$ ion signal using the linear relationship between the $\text{F}_2^{34}\text{SO}_2^-$ ion sensitivity
416 and ambient water vapor concentration (Fig. S2c) in our post-field calibrations, where the
417 response of the CIMS acid signals were measured relative to the of the $^{34}\text{SO}_2$ sensitivity.

418 3.1.3. Background and calibration measurements

419 Figure S4 shows an example of the CIMS instrument response during the switch
420 between background, calibration and ambient measurements of formic and acetic acids
421 during the field study. The 13 s time resolution data was used to determine the CIMS
422 instrument time response. Formic (m/z 45, 65 and 108) and acetic (m/z 79) acid ion signals
423 took ~1.5 min to reach a steady state after switches between ambient, calibration and
424 background measurements (Figs. S4a and S4c).

425 The CIMS time response to a compound is governed primarily by the compound's
426 propensity to adhere to surfaces. The decays in the formic and acetic acid ion signals and
427 times required for them to reach steady state after the removal of calibration gases during
428 the switch from standard addition calibration to ambient sampling were used to determine
429 the CIMS response time. The signal decays were fitted using double exponential functions.
430 For formic acid, the m/z 45, 65 and 108 ion signals decayed to $1/e^2$ in 37 ± 2 , 33 ± 2 and
431 32 ± 2 s, respectively (Fig. S4b). For acetic acid, the m/z 79 ion signal decayed to $1/e^2$ in
432 42 ± 2 s (Fig. S4d).

433 **3.2. Ambient measurements**

434 **3.2.1. Formic acid**

435 Figure 2 shows typical mass spectra obtained under background and measurement
436 modes during the field study. The SF_6^- reagent ion is present at m/z 146. One of the
437 prominent species in the mass spectrum is formic acid, which is detected as $HCOO^-$ and
438 $HCOO \cdot HF$ at m/z 45 and 65, respectively. Our laboratory studies demonstrated that the
439 reaction of formic acid with SF_6^- also produced a large fraction of SF_4^- ions at m/z 108.
440 The reaction of SF_6^- with oxalic acid also produced SF_4^- ions, but its SF_4^- product ion yield
441 is low and gas phase oxalic acid is not present in large concentrations. In addition, SF_4^- is
442 present in the mass spectrum obtained under background mode but the SF_4^- background
443 ion signals are lower than those typically observed in measurement mode at the Yorkville
444 site. As a result, we determined the ambient formic acid concentrations using the $HCOO^-$,
445 $HCOO \cdot HF$ and SF_4^- ions. Figure 3a shows a scatter plot comparing the ambient formic
446 acid concentrations measured at Yorkville using the $HCOO^-$, $HCOO \cdot HF$ and SF_4^- ions.
447 Linear regression analysis reveals that the formic acid concentrations determined by the

448 three ions are highly correlated ($R^2 = 0.99$) with slopes exhibiting a near 1:1 correlation.
449 The excellent correlation between these three ions and the agreement with laboratory data
450 indicates that formic acid is selectively measured by this method.

451 The time series of formic acid, temperature and solar radiation measured at
452 Yorkville are shown in Fig. 3b. Formic acid concentrations ranged from 40 ppt to 4 ppb
453 during the field study, with strong and consistent diurnal trends. The day-to-day variability
454 in formic acid concentrations are associated with changes in solar radiation and
455 temperature. Higher formic acid concentrations are measured during warm and sunny days,
456 similar to formic acid measurements performed in Centreville, rural Alabama during the
457 2013 Southern Oxidant Aerosol Study (SOAS) (Brophy and Farmer, 2015; Millet et al.,
458 2015). Figure 3c shows the study-averaged diurnal profiles of formic acid and solar
459 irradiance. Formic acid started to increase at 7:30, which coincided with a sharp increase
460 in solar irradiance. Concentrations continued to increase throughout the day and peaked at
461 18:30, which coincided with the approximate time just before solar irradiance reached zero.
462 Formic acid then decreased continuously throughout the night.

463 The immediate early-morning increase in formic acid observed in this field study
464 is similar to that seen during the SOAS study (Millet et al., 2015). However, there are some
465 differences in the formic acid diurnal cycles measured in this field study and the SOAS
466 study. Formic acid peaked at 15:30 during SOAS, approximately 3 hours before solar
467 irradiance decreased to zero. In contrast, formic acid concentrations only started to
468 decrease at sunset (at 19:30) in this study. This suggests that there may be differences in
469 the types and/or magnitudes of formic acid sources and sinks in this two field studies. Land
470 cover and/or land use differences may have contributed to differences in formic acid
471 sources and sinks at the Centreville and Yorkville field sites. The area surrounding the
472 Yorkville field site is covered primarily by hardwood mixed with farmland and open
473 pastures. In contrast, the Centreville field site is surrounded by forests comprised of mixed
474 oak-hickory and loblolly trees (Hansen et al., 2003). It is also possible that seasonal
475 differences contributed to differences in formic acid sources and sinks in the two field
476 studies. The SOAS campaign took place in the middle of summer (1 June to 15 July 2013)
477 when biogenic emissions are typically higher while this field study took place in early fall

478 when biogenic emissions are lower due to cooler temperatures. For example, the average
479 concentration of isoprene (a formic acid source) in this study (1.21 ppb) is lower than that
480 in SOAS (1.92 ppb (Millet et al., 2015)). Despite these differences, our overall results are
481 similar to the formic acid measurements performed in SOAS in both magnitude and diurnal
482 variability.

483 3.2.2. Acetic acid

484 Acetic acid is detected with SF_6^- as CH_3COO^- and $\text{CH}_3\text{COO}^-\cdot\text{HF}$ at m/z 59 and 79,
485 respectively. However, these ions are subject to interferences from the reaction of SF_6^- with
486 water vapor present in the sampled ambient air. Two of these interfering ions $\text{F}^-\cdot(\text{HF})_2$ and
487 $\text{F}^-\cdot(\text{HF})_3$ occur at m/z 59 and 79, respectively. As discussed earlier, we minimized the
488 impact of these interferences by diluting the sample flow into the CIMS and running the
489 CDC at a high collision energy to dissociate the HF cluster ions. As expected from cluster
490 bond strengths, we found that larger HF cluster ions dissociated more easily than smaller
491 ones. For example, at a CDC electric field of $\sim 113 \text{ V cm}^{-1}$ (the configuration used in this
492 field study), virtually all of the $\text{F}^-\cdot(\text{HF})_3$ cluster ions dissociated while very few of the $\text{F}^-\cdot$
493 $\cdot(\text{HF})$ cluster ions dissociated. This indicates that the m/z 79 channel for acetic acid is more
494 immune to interference from water vapor than the m/z 59 channel. This is supported by the
495 observation that the background ion signal at m/z 59 ($R^2 = 0.50$) is more highly correlated
496 with ambient water vapor concentrations than the background ion signal of m/z 79 ($R^2 =$
497 0.30). In addition, the m/z 59 ion is subjected to interference from the reaction of SF_6^- with
498 O_3 present in the sampled ambient air. SF_6^- reacts with O_3 in the presence of CO_2 to form
499 CO_3^- at m/z 60 (Slusher et al., 2001). As shown in Fig. 2, the large CO_3^- peak at m/z 60 is
500 a potential interference to the m/z 59 signal. As the background scrubber also removed O_3
501 from the ambient air, there is a large difference in the m/z 60 ion signal between the
502 measurement and background modes ($\sim 100\,000 \text{ Hz}$). Thus, even a few percent bleed over
503 of m/z 60 to m/z 59 can lead to an over-estimation of ambient acetic acid concentrations.
504 For these reasons, we used m/z 79 ($\text{X}^-\cdot\text{HF}$) to determine ambient acetic acid concentrations
505 even though this channel has a lower sensitivity than the m/z 59 channel (X^-).

506 The time series of acetic acid, temperature and solar radiation measured at
507 Yorkville are shown in Fig. 4a. Acetic acid concentrations ranged from 30 ppt to 3 ppb

508 during the field study. The day-to-day variability in acetic acid concentrations resembled
509 the behavior of formic acid concentrations, with higher concentrations being measured
510 during warm and sunny days. Figure 4b shows the study-averaged diurnal profiles of acetic
511 acid and solar irradiance. The diurnal profile of acetic acid is similar to that of formic acid
512 with a more pronounced evening maximum. Acetic acid started to increase at 7:30 and
513 built up through the day, peaking at 19:30 and decreased continuously overnight. In
514 general, acetic acid concentrations are well correlated with ($R^2 = 0.67$) and comparable in
515 magnitude (~60 % on average) to formic acid. The study-averaged formic acid/acetic acid
516 concentration ratio (1.65) is comparable to ratios from previous field studies in rural and
517 urban environments (Talbot et al., 1988; Talbot et al., 1995; Granby et al., 1997; Khare et
518 al., 1999; Talbot et al., 1999; Baboukas et al., 2000; Singh et al., 2000; Kuhn et al., 2002;
519 Baasandorj et al., 2015; Millet et al., 2015).

520 **3.2.3. Larger organic acids**

521 In addition to formic and acetic acid, eight other ions were monitored during the
522 field study: m/z 73, 75, 87, 89, 101, 103, 117 and 131. These ions were chosen as they had
523 significant signals when ambient air was sampled and were not obviously formed from
524 SF_6^- reaction with water vapor or O_3 . Since the CIMS utilized in this study only had unit
525 mass resolution, these ions are the sum of all organic acid isomers and isobaric organic
526 acids of the same molecular weight as well as other product ions from species that might
527 react with SF_6^- . We will refer to organic acids with m/z 75, 87, 101, 103, 117 and 131 by
528 their ion masses. We assign the m/z 73 ion as the X^- ion of propionic acid because it does
529 not have organic acid isomers and isobaric species at that m/z. In addition, real-time ion
530 chromatography measurements of aerosol composition performed during the field study
531 demonstrated the presence of particulate oxalic acid (Nah et al., 2018). For this reason, we
532 assign the m/z 89 ion as the X^- ion of oxalic acid. As shown in Nah et al. (2018), the gas-
533 particle ratios of the organic acids depend of their thermodynamic conditions, which are
534 dependent on the acid's physicochemical properties, ambient temperature, particle water
535 and pH. Since the measured gas-particle partitioning ratios of oxalic acid (calculated using
536 the CIMS and ion chromatography measurements) are in good agreement with their
537 corresponding thermodynamic predictions (Nah et al., 2018), this indicated that our

538 assignment of the m/z 89 ion to oxalic acid is reasonable. In addition, the high sensitivity
539 of SF₆⁻ to oxalic acid also helps limit interferences due to other acids. Particulate formic
540 acid and acetic acid were also detected by ion chromatography during the field study, but
541 were at much lower concentrations relative to the gas phase (Nah et al., 2018).

542 Figures 5 and S5 show the time series and diurnal profiles of oxalic and propionic
543 acids and organic acids with ions m/z 75, 87, 101, 103, 117 and 131 measured during the
544 field study. These organic acids displayed very similar day-to-day variability as formic and
545 acetic acids, with higher concentrations (or ion signals) being measured on warm and sunny
546 days. The diurnal profiles of all the measured organic acids have similar diurnal trends,
547 with their concentrations (or ion signals) reaching a maximum between 17:30 and 19:30
548 and rapidly decreasing after sunset.

549 **3.2.4. Comparison with WSOC_g**

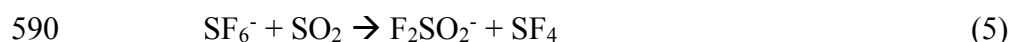
550 WSOC_g measurements were performed during the field study using a MIST
551 chamber coupled to a TOC analyzer. The study average WSOC_g was $3.6 \pm 2.7 \mu\text{gC m}^{-3}$,
552 slightly lower than that measured during the SOAS study ($4.9 \mu\text{gC m}^{-3}$) (Xu et al., 2017),
553 and approximately four times lower than that measured in urban Atlanta, Georgia (13.7
554 $\mu\text{gC m}^{-3}$) (Hennigan et al., 2009). Despite being comparable in magnitude, the diurnal
555 profiles of WSOC_g measured in this study and the SOAS study are different. WSOC_g
556 measured in the SOAS study decreased at sunset, while WSOC_g measured in this study
557 decreased 2 hours after sunset. Differences in WSOC_g concentrations and diurnal profiles
558 at the three different sites may be due to differences in emission sources as a result of
559 different measurement periods, land use and/or land cover.

560 To estimate the fraction of WSOC_g that is comprised of organic acids, the total
561 organic carbon contributed by formic, acetic, oxalic and propionic acids is compared to the
562 WSOC_g measurements. This comparison primarily serves as a check to determine if the
563 peak assignments are plausible by ensuring that the estimated sum of organic carbon
564 contributed by these four organic acids is less than or equal to the measured WSOC_g.
565 Figures 6a and 6b show the time series and diurnal profiles of WSOC_g and the organic
566 carbon contributed by the four organic acids. Formic and acetic acids comprised majority

567 of the total organic carbon contributed by the four organic acids (study averages of 41 and
568 54 %, respectively). The carbon mass fraction of WSOC_g comprised of these four organic
569 acids ranged from 2 to 100 %. Based on the orthogonal distance regression slope shown in
570 Fig. 6c, the study-averaged carbon mass fraction of WSOC_g comprised of the four organic
571 acids is 22 %. The total organic carbon contributed by the four organic acids are moderately
572 correlated with WSOC_g ($R^2 = 0.42$). This is likely due to the presence of other water-soluble
573 gas phase species (with different day-to-day variability from the organic acids) that
574 contribute to the WSOC_g. This is supported by slight differences in the diurnal profiles of
575 WSOC_g and the organic carbon contributed by the organic acids (Fig. 6b). While the
576 diurnal profiles of WSOC_g and the organic carbon contributed by the four organic acids
577 have similar general shapes, WSOC_g peaked at 21:30, approximately 2 hours after the solar
578 irradiance have decreased to zero. In contrast, the organic carbon contributed by the four
579 organic acids start to decrease at sunset (at 19:30).

580 3.2.5. SO₂ and HNO₃ observations

581 In addition to evaluating the field performance of the SF₆⁻ CIMS technique in gas-
582 phase organic acid measurements, another focus of this study was to investigate the
583 possible sources of the measured organic acids. For this reason, HNO₃ and SO₂ (two
584 common anthropogenic tracers) were also measured by SF₆⁻ CIMS during the field study.
585 Correlations between the concentrations of organic acids and those of HNO₃ and SO₂ were
586 then examined to determine if the organic acids were anthropogenic in nature (section 3.3).
587 While their reactions with SF₆⁻ have multiple product channels (Huey et al., 1995), only
588 the NO₃⁻•HF (m/z 82) and F₂SO₂⁻ (m/z 102) ions were used for quantitative purposes:



591 Figure S6 shows the time series of SO₂ and HNO₃ measured during the field study.
592 As expected at a rural site, SO₂ and HNO₃ concentrations are low most of the time (study
593 averages of 230 and 180 ppt, respectively). However, there were occasional periods when
594 the site was impacted by anthropogenic pollution. In particular, there are spikes in both
595 SO₂ and HNO₃ concentrations lasting between 1 to 3 hours throughout the study that

596 corresponded to the site being impacted by power plant or urban emissions. Outside of
597 these anthropogenic spikes, HNO₃ showed a clear diurnal profile with a maximum at
598 approximately 12:30, consistent with local photochemical production.

599 **3.3. Potential sources of organic acids**

600 Correlation analysis on organic acid concentrations can provide insights on their
601 sources. Figure 7 shows that the concentration of formic acid is strongly correlated with
602 those of the other measured organic acids ($R^2 = 0.68$ to 0.89). This suggests that these
603 organic acids have the same or similar sources at Yorkville. The sources of organic acids
604 can be biogenic or anthropogenic in nature. To determine if the primary sources of organic
605 acids are of biogenic or anthropogenic origin, we first examined the correlations of organic
606 acid concentrations with those of anthropogenic pollutants CO, SO₂, O₃ and HNO₃. CO
607 and SO₂ are common tracers for combustion sources. The organic acid concentrations (or
608 ion signals) are poorly correlated with CO (Fig. S7, $R^2 = 0.04$ to 0.15) and SO₂ (Fig. S8,
609 $R^2 = 0.01$ to 0.23), indicating that primary emissions from combustion are a minor source
610 of organic acids in Yorkville. HNO₃ and O₃ are common photochemical tracers of urban
611 air masses. The organic acid concentrations (or ion signals) are weakly correlated with O₃
612 (Fig. S9, $R^2 = 0.11$ to 0.31) and HNO₃ (Fig. S10, $R^2 = 0.33$ to 0.60). In addition, there is
613 no noticeable increase in organic acid concentrations during periods of elevated CO, SO₂,
614 O₃ and HNO₃ concentrations when the site was impacted by pollution plumes. Formic
615 acid/CO ratios (which have been used in some studies to determine the contribution of
616 polluted air masses) ranged between 1.0×10^{-3} to 2.5×10^{-2} ppb ppb⁻¹. The ratio peaked
617 consistently in the mid-afternoon, which coincided with when formic acid and CO reached
618 their maximum and minimum, respectively. In addition, there were no spikes in the formic
619 acid/CO ratio during the study, suggesting that contributions of polluted air masses to the
620 daily increase in formic acid are minimal. Together, these results indicate that the primary
621 sources of organic acids in Yorkville are likely not anthropogenic in nature.

622 Diurnal profiles of the measured organic acids suggest that their sources are linked
623 to higher daytime temperatures and/or photochemical processes. Figure 8 compares the
624 concentrations (or ion signals) of organic acids against ambient temperatures measured
625 during the study. Since there was a noticeable decrease in mean ambient temperatures

626 starting on 28 Sept 2016, we grouped the datasets into two time periods (3 to 27 Sept and
627 28 Sept to 12 Oct) to better evaluate the effect of temperature on organic acid
628 concentrations. The average temperature in the first time period (3 to 27 Sept) is 24.8 °C
629 (32.6 °C max, 18.1 °C min), while the average temperature in the second time period (28
630 Sept to 12 Oct) is 19.5 °C (28.4 °C max, 9.5 °C min). We find that organic acid
631 concentrations are on average higher and more highly correlated with temperatures in the
632 warmer first time period ($R^2 = 0.40$ to 0.61) compared to the cooler second time period (R^2
633 $= 0.18$ to 0.55). These observations can be explained by temperature-dependent emissions
634 of organic acids and their BVOC precursors. Previous studies have shown that emissions
635 of organic acids and their BVOC precursors depend strongly on light and temperature, with
636 substantially lower concentrations being emitted in the dark and/or at low temperatures
637 (Kesselmeier et al., 1997; Kesselmeier, 2001; Sindelarova et al., 2014). We find that the
638 concentration of isoprene, which was the dominant BVOC in Yorkville, has a somewhat
639 similar diurnal profile as the organic acids and decreased with temperature on 28 Sept 2016
640 (Fig. S11). In addition, the concentrations of formic and acetic acids are moderately
641 correlated with that of isoprene ($R^2 = 0.42$ and 0.40 , respectively) (Fig. S12).

642 Multiphase photochemical aging of ambient organic aerosols can also be a source
643 of gas-phase organic acids (Eliason et al., 2003; Ervens et al., 2004; Molina et al., 2004;
644 Lim et al., 2005; Park et al., 2006; Walser et al., 2007; Sorooshian et al., 2007; Vlasenko
645 et al., 2008; Pan et al., 2009; Sorooshian et al., 2010). Organic acids may be formed in the
646 particle phase during organic aerosol photochemical aging, with subsequent volatilization
647 into the gas phase. Real-time ion chromatography measurements of aerosol composition
648 demonstrated the presence of particulate formic, acetic, oxalic, malonic, succinic and
649 glutaric acids (Nah et al., 2018). However, since the ratios of gas-phase formic and acetic
650 acid mass concentration to the total organic aerosol mass concentration are large (study
651 averages of 40 and 35 %, respectively) (Nah et al., 2018), it is unlikely that organic aerosol
652 photochemical aging is a large source of formic and acetic acids. In contrast, the ratios of
653 gas-phase oxalic, malonic, succinic and glutaric acids mass concentration to the total
654 organic aerosol mass concentration are expected to be small, suggesting that organic
655 aerosol photochemical aging may be an important source of these gas-phase organic acids.

656 In summary, the temperature dependence and diurnal profile of organic acid
657 concentrations combined with poor correlations between organic acid concentrations and
658 those of anthropogenic pollutants CO, SO₂, O₃ and HNO₃ strongly suggest that the primary
659 sources of gas-phase organic acids at Yorkville are biogenic in nature. However, our data
660 alone does not allow us to determine if the organic acids are a result of direct emissions or
661 photochemical oxidation of other BVOC emissions and/or organic aerosols. Partitioning
662 of these organic acids between the gas and particle phases is discussed in another paper
663 (Nah et al., 2018).

664 **4. Summary**

665 SF₆⁻ reacted with all of the studied organic acids to produce product ions that were
666 characteristic of the individual acids (i.e., X⁻ or X⁻•HF). These reactions all occurred at less
667 than the maximum collisional rate due to significant yields of SF₅⁻ and SF₄⁻, which reduced
668 the sensitivity of the method. For the conditions employed in this study, the sensitivities of
669 X⁻ and X⁻•HF ions of the organic acids ranged from 0.12 to 6.38 Hz ppt⁻¹. The detection
670 limits of the organic acids were approximated from 3 times the standard deviation values
671 (3σ) of the ion signals obtained during background measurements. Limits of detection
672 ranged from 1 to 60 ppt for 2.5 min integration periods for the organic acids studied. It
673 should be noted that the SF₆⁻ CIMS method is particularly sensitive to oxalic, propionic
674 and glycolic acids, which are expected to be present at low concentrations in the
675 atmosphere. Water vapor and O₃ can lead to interferences with this method but for the
676 conditions employed in this study, they were largely limited to acetic acid measurements
677 at m/z 59. However, fluctuations in ambient water vapor can also lead to changes in
678 sensitivity for the detection of some species (e.g., SO₂). Uncertainties in organic acid
679 concentrations originate primarily from calibration measurements and ranged from 12 to
680 14 %. Overall, the tractable mass spectra obtained by the SF₆⁻ CIMS method coupled with
681 reasonable limits of detection and the high correlations observed between the individual
682 organic acids demonstrated the potential of this method. Obvious next steps for the SF₆⁻
683 CIMS method are to compare it to other measurement methods for organic acids and to
684 deploy the SF₆⁻ ion chemistry to a higher resolution time-of-flight mass spectrometer to
685 reduce the potential for interferences.

686 The SF₆⁻ CIMS method was deployed for measurements of gas phase organic acids
687 in a mixed forest-agricultural area in Yorkville, Georgia from Sept to Oct 2016. The
688 organic acids measured in the field study were formic, acetic, propionic and oxalic acids.
689 Ambient concentrations of these organic acids ranged from a few ppt to several ppb. All
690 the organic acids exhibited similar strong diurnal trends. Organic acid concentrations built
691 up throughout the day, peaked between 17:30 and 19:30 before decreasing continuously
692 overnight. Strong correlations between organic acid concentrations indicated that these
693 organic acids likely have the same or similar sources at Yorkville. We concluded that the
694 organic acids were likely not due to anthropogenic emissions since they were poorly
695 correlated with anthropogenic pollutants and their concentrations were not elevated when
696 the site was impacted by pollution plumes. Higher organic acid concentrations were
697 measured during warm and sunny days. Organic acid concentrations were strongly
698 correlated with temperature during the first month of the study when ambient temperatures
699 were high. Together, our results suggested that the primary sources of organic acids at
700 Yorkville were biogenic in nature. Direct biogenic emissions of organic acids and/or their
701 BVOC precursors were likely enhanced at high ambient temperatures, resulting in the
702 observed variability of organic acid concentrations. Another potential source is the
703 production of organic acids in the particle phase from the multiphase photochemical aging
704 of organic aerosols followed by evaporation to the gas phase, though this source is likely
705 not a large source of formic and acetic acids. However, given the inability of current models
706 and photochemical mechanisms to explain formic acid observations in the Southeastern
707 U.S. (Millet et al., 2015), it is unlikely that our observations of formic acid and larger
708 organic acids can be explained as well. Further work (i.e., laboratory, field and modeling
709 studies) is needed to determine how organic acids are formed in the atmosphere.

710 **5. Acknowledgements**

711 The authors thank Eric Edgerton (Atmospheric Research and Analysis, Inc.) for
712 providing CO, O₃ and VOC measurements and meteorological data.

713 **6. Funding**

714 This publication was developed under US Environmental Protection Agency (EPA)
715 STAR Grant R835882 awarded to Georgia Institute of Technology. It has not been
716 formally reviewed by the EPA. The views expressed in this document are solely those of
717 the authors and do not necessarily reflect those of the EPA. EPA does not endorse any
718 products or commercial services mentioned in this publication.

719 **7. Competing financial interests**

720 The authors declare no competing financial interests.

721 **8. Data availability**

722 Data can be accessed by request (greg.huey@eas.gatech.edu).

723 **9. References**

724 Acree, W., and Chickos, J. S.: Phase Transition Enthalpy Measurements of Organic and
725 Organometallic Compounds. Sublimation, Vaporization and Fusion Enthalpies From 1880
726 to 2010, *J. Phys. Chem. Ref. Data*, 39, 942, 10.1063/1.3309507, 2010.

727 Aljawhary, D., Lee, A. K. Y., and Abbatt, J. P. D.: High-resolution chemical ionization
728 mass spectrometry (ToF-CIMS): application to study SOA composition and processing,
729 *Atmospheric Measurement Techniques*, 6, 3211-3224, 10.5194/amt-6-3211-2013, 2013.

730 Andreae, M. O., Talbot, R. W., Andreae, T. W., and Harriss, R. C.: Formic and Acetic
731 Acid over the Central Amazon Region, Brazil. 1. Dry Season, *Journal of Geophysical
732 Research-Atmospheres*, 93, 1616-1624, 10.1029/JD093iD02p01616, 1988.

733 Arnold, S. T., and Viggiano, A. A.: Turbulent ion flow tube study of the cluster-mediated
734 reactions of SF₆⁻ with H₂O, CH₃OH, and C₂H₅OH from 50 to 500 torr, *J. Phys. Chem.
735 A*, 105, 3527-3531, 10.1021/jp003967y, 2001.

736 Baasandorj, M., Millet, D. B., Hu, L., Mitroo, D., and Williams, B. J.: Measuring acetic
737 and formic acid by proton-transfer-reaction mass spectrometry: sensitivity, humidity
738 dependence, and quantifying interferences, *Atmospheric Measurement Techniques*, 8,
739 1303-1321, 10.5194/amt-8-1303-2015, 2015.

740 Baboukas, E. D., Kanakidou, M., and Mihalopoulos, N.: Carboxylic acids in gas and
741 particulate phase above the Atlantic Ocean, *Journal of Geophysical Research-*
742 *Atmospheres*, 105, 14459-14471, 10.1029/1999jd900977, 2000.

743 Booth, A. M., Barley, M. H., Topping, D. O., McFiggans, G., Garforth, A., and Percival,
744 C. J.: Solid state and sub-cooled liquid vapour pressures of substituted dicarboxylic acids
745 using Knudsen Effusion Mass Spectrometry (KEMS) and Differential Scanning
746 Calorimetry, *Atmos. Chem. Phys.*, 10, 4879-4892, 10.5194/acp-10-4879-2010, 2010.

747 Brophy, P., and Farmer, D. K.: A switchable reagent ion high resolution time-of-flight
748 chemical ionization mass spectrometer for real-time measurement of gas phase oxidized
749 species: characterization from the 2013 southern oxidant and aerosol study, *Atmospheric*
750 *Measurement Techniques*, 8, 2945-2959, 10.5194/amt-8-2945-2015, 2015.

751 Carlton, A. G., Turpin, B. J., Lim, H. J., Altieri, K. E., and Seitzinger, S.: Link between
752 isoprene and secondary organic aerosol (SOA): Pyruvic acid oxidation yields low volatility
753 organic acids in clouds, *Geophys. Res. Lett.*, 33, 4, 10.1029/2005gl025374, 2006.

754 Chebbi, A., and Carlier, P.: Carboxylic acids in the troposphere, occurrence, sources, and
755 sinks: A review, *Atmospheric Environment*, 30, 4233-4249, 10.1016/1352-
756 2310(96)00102-1, 1996.

757 Crounse, J. D., McKinney, K. A., Kwan, A. J., and Wennberg, P. O.: Measurement of gas-
758 phase hydroperoxides by chemical ionization mass spectrometry, *Analytical Chemistry*,
759 78, 6726-6732, 10.1021/ac0604235, 2006.

760 Daubert, T. E., and Danner, R. P.: Physical and thermodynamic properties of pure
761 chemicals: data compilation, Taylor & Francis, Washington, DC, 1989.

762 Eliason, T. L., Aloisio, S., Donaldson, D. J., Cziczo, D. J., and Vaida, V.: Processing of
763 unsaturated organic acid films and aerosols by ozone, *Atmospheric Environment*, 37, 2207-
764 2219, 10.1016/s1352-2310(03)00149-3, 2003.

765 Ervens, B., Feingold, G., Frost, G. J., and Kreidenweis, S. M.: A modeling study of aqueous
766 production of dicarboxylic acids: 1. Chemical pathways and speciated organic mass

767 production, *Journal of Geophysical Research-Atmospheres*, 109, 10.1029/2003jd004387,
768 2004.

769 Ervens, B., Carlton, A. G., Turpin, B. J., Altieri, K. E., Kreidenweis, S. M., and Feingold,
770 G.: Secondary organic aerosol yields from cloud-processing of isoprene oxidation
771 products, *Geophys. Res. Lett.*, 35, 10.1029/2007gl031828, 2008.

772 Galloway, J. N., Likens, G. E., Keene, W. C., and Miller, J. M.: The Composition of
773 Precipitation in Remote Areas of the World, *Journal of Geophysical Research-Oceans and*
774 *Atmospheres*, 87, 8771-8786, 10.1029/JC087iC11p08771, 1982.

775 Granby, K., Egelov, A. H., Nielsen, T., and Lohse, C.: Carboxylic acids: Seasonal variation
776 and relation to chemical and meteorological parameters, *Journal of Atmospheric*
777 *Chemistry*, 28, 195-207, 10.1023/a:1005877419395, 1997.

778 Grosjean, D.: Ambient Levels of Formaldehyde, Acetaldehyde, and Formic acid in
779 Southern Californic- Results of a One-year Base-line Study, *Environmental Science &*
780 *Technology*, 25, 710-715, 10.1021/es00016a016, 1991.

781 Hansen, D. A., Edgerton, E. S., Hartsell, B. E., Jansen, J. J., Kandasamy, N., Hidy, G. M.,
782 and Blanchard, C. L.: The southeastern aerosol research and characterization study: Part 1-
783 overview, *Journal of the Air & Waste Management Association*, 53, 1460-1471, 2003.

784 Hartmann, W. R., Santana, M., Hermoso, M., Andreae, M. O., and Sanhueza, E.: Diurnal
785 Cycles of Formic and Acetic Acids in the Northern Part of the Guayana Sheld, Venezuela,
786 *Journal of Atmospheric Chemistry*, 13, 63-72, 10.1007/bf00048100, 1991.

787 Hennigan, C. J., Bergin, M. H., Russell, A. G., Nenes, A., and Weber, R. J.: Gas/particle
788 partitioning of water-soluble organic aerosol in Atlanta, *Atmos. Chem. Phys.*, 9, 3613-
789 3628, 10.5194/acp-9-3613-2009, 2009.

790 Huey, L. G., Hanson, D. R., and Howard, C. J.: Reactions of SF₆- and I- with Atmospheric
791 Trace Gases, *Journal of Physical Chemistry*, 99, 5001-5008, 10.1021/j100014a021, 1995.

792 Huey, L. G., Tanner, D. J., Slusher, D. L., Dibb, J. E., Arimoto, R., Chen, G., Davis, D.,
793 Buhr, M. P., Nowak, J. B., Mauldin, R. L., Eisele, F. L., and Kosciuch, E.: CIMS
794 measurements of HNO₃ and SO₂ at the South Pole during ISCAT 2000, *Atmospheric*
795 *Environment*, 38, 5411-5421, 10.1016/j.atmosenv.2004.04.037, 2004.

796 Kawamura, K., Ng, L. L., and Kaplan, I. R.: Determination of Organic Acids (C1-C10) in
797 the Atmosphere, Motor Exhausts, and Engine Oils, *Environmental Science & Technology*,
798 19, 1082-1086, 10.1021/es00141a010, 1985.

799 Keene, W. C., Galloway, J. N., and Holden, J. D.: Measurement of Weak Organic Acidity
800 in Precipitation from Remote Areas of the World, *Journal of Geophysical Research-Oceans*
801 *and Atmospheres*, 88, 5122-5130, 10.1029/JC088iC09p05122, 1983.

802 Keene, W. C., and Galloway, J. N.: Organic Acidity in Precipitation of North America,
803 *Atmospheric Environment*, 18, 2491-2497, 10.1016/0004-6981(84)90020-9, 1984.

804 Kesselmeier, J., Bode, K., Hofmann, U., Muller, H., Schafer, L., Wolf, A., Ciccioli, P.,
805 Brancaleoni, E., Cecinato, A., Frattoni, M., Foster, P., Ferrari, C., Jacob, V., Fugit, J. L.,
806 Dutaur, L., Simon, V., and Torres, L.: Emission of short chained organic acids, aldehydes
807 and monoterpenes from *Quercus ilex* L. and *Pinus pinea* L. in relation to physiological
808 activities, carbon budget and emission algorithms, *Atmospheric Environment*, 31, 119-133,
809 10.1016/s1352-2310(97)00079-4, 1997.

810 Kesselmeier, J.: Exchange of short-chain oxygenated volatile organic compounds (VOCs)
811 between plants and the atmosphere: A compilation of field and laboratory studies, *Journal*
812 *of Atmospheric Chemistry*, 39, 219-233, 10.1023/a:1010632302076, 2001.

813 Khare, P., Kumar, N., Kumari, K. M., and Srivastava, S. S.: Atmospheric formic and acetic
814 acids: An overview, *Reviews of Geophysics*, 37, 227-248, 10.1029/1998rg900005, 1999.

815 Kim, S., Huey, L. G., Stickel, R. E., Tanner, D. J., Crawford, J. H., Olson, J. R., Chen, G.,
816 Brune, W. H., Ren, X., Leshner, R., Wooldridge, P. J., Bertram, T. H., Perring, A., Cohen,
817 R. C., Lefer, B. L., Shetter, R. E., Avery, M., Diskin, G., and Sokolik, I.: Measurement of
818 HO₂NO₂ in the free troposphere during the intercontinental chemical transport experiment

819 - North America 2004, *Journal of Geophysical Research-Atmospheres*, 112,
820 10.1029/2006jd007676, 2007.

821 Kuhn, U., Rottenberger, S., Biesenthal, T., Ammann, C., Wolf, A., Schebeske, G., Oliva,
822 S. T., Tavares, T. M., and Kesselmeier, J.: Exchange of short-chain monocarboxylic acids
823 by vegetation at a remote tropical forest site in Amazonia, *Journal of Geophysical*
824 *Research-Atmospheres*, 107, 18, 10.1029/2000jd000303, 2002.

825 Lee, B. H., Lopez-Hilfiker, F. D., Mohr, C., Kurten, T., Worsnop, D. R., and Thornton, J.
826 A.: An Iodide-Adduct High-Resolution Time-of-Flight Chemical-Ionization Mass
827 Spectrometer: Application to Atmospheric Inorganic and Organic Compounds,
828 *Environmental Science & Technology*, 48, 6309-6317, 10.1021/es500362a, 2014.

829 Liao, J., Sihler, H., Huey, L. G., Neuman, J. A., Tanner, D. J., Friess, U., Platt, U., Flocke,
830 F. M., Orlando, J. J., Shepson, P. B., Beine, H. J., Weinheimer, A. J., Sjostedt, S. J., Nowak,
831 J. B., Knapp, D. J., Staebler, R. M., Zheng, W., Sander, R., Hall, S. R., and Ullmann, K.:
832 A comparison of Arctic BrO measurements by chemical ionization mass spectrometry and
833 long path-differential optical absorption spectroscopy, *Journal of Geophysical Research-*
834 *Atmospheres*, 116, 10.1029/2010jd014788, 2011.

835 Lide, D. R.: *CRC handbook of chemistry and physics: a ready-reference book of chemical*
836 *and physical data*, CRC Press, Boca Raton, FL, 1995.

837 Lim, H. J., Carlton, A. G., and Turpin, B. J.: Isoprene forms secondary organic aerosol
838 through cloud processing: Model simulations, *Environmental Science & Technology*, 39,
839 4441-4446, 10.1021/es048039h, 2005.

840 Millet, D. B., Baasandorj, M., Farmer, D. K., Thornton, J. A., Baumann, K., Brophy, P.,
841 Chaliyakunnel, S., de Gouw, J. A., Graus, M., Hu, L., Koss, A., Lee, B. H., Lopez-Hilfiker,
842 F. D., Neuman, J. A., Paulot, F., Peischl, J., Pollack, I. B., Ryerson, T. B., Warneke, C.,
843 Williams, B. J., and Xu, J.: A large and ubiquitous source of atmospheric formic acid,
844 *Atmos. Chem. Phys.*, 15, 6283-6304, 10.5194/acp-15-6283-2015, 2015.

845 Molina, M. J., Ivanov, A. V., Trakhtenberg, S., and Molina, L. T.: Atmospheric evolution
846 of organic aerosol, *Geophys. Res. Lett.*, 31, 10.1029/2004gl020910, 2004.

847 Nah, T., Guo, H., Sullivan, A. P., Chen, Y., Tanner, D. J., Nenes, A., Russell, A., Ng, N.
848 L., Huey, L. G., and Weber, R. J.: Characterization of Aerosol Composition, Aerosol
849 Acidity and Organic Acid Partitioning at an Agriculture-intensive Rural Southeastern U.S.
850 Site, *Atmos. Chem. Phys. Discuss.*, in review, 10.5194/acp-2018-373, 2018.

851 Neuman, J. A., Ryerson, T. B., Huey, L. G., Jakoubek, R., Nowak, J. B., Simons, C., and
852 Fehsenfeld, F. C.: Calibration and evaluation of nitric acid and ammonia permeation tubes
853 by UV optical absorption, *Environmental Science & Technology*, 37, 2975-2981,
854 10.1021/es0264221, 2003.

855 Nguyen, T. B., Crouse, J. D., Teng, A. P., Clair, J. M. S., Paulot, F., Wolfe, G. M., and
856 Wennberg, P. O.: Rapid deposition of oxidized biogenic compounds to a temperate forest,
857 *Proc. Natl. Acad. Sci. U. S. A.*, 112, E392-E401, 10.1073/pnas.1418702112, 2015.

858 Nolte, C. G., Solomon, P. A., Fall, T., Salmon, L. G., and Cass, G. R.: Seasonal and spatial
859 characteristics of formic and acetic acids concentrations in the southern California
860 atmosphere, *Environmental Science & Technology*, 31, 2547-2553, 10.1021/es960954i,
861 1997.

862 Nowak, J. B., Huey, L. G., Russell, A. G., Tian, D., Neuman, J. A., Orsini, D., Sjostedt, S.
863 J., Sullivan, A. P., Tanner, D. J., Weber, R. J., Nenes, A., Edgerton, E., and Fehsenfeld, F.
864 C.: Analysis of urban gas phase ammonia measurements from the 2002 Atlanta Aerosol
865 Nucleation and Real-Time Characterization Experiment (ANARChE), *Journal of*
866 *Geophysical Research-Atmospheres*, 111, 14, 10.1029/2006jd007113, 2006.

867 Orzechowska, G. E., and Paulson, S. E.: Photochemical sources of organic acids. 1.
868 Reaction of ozone with isoprene, propene, and 2-butenes under dry and humid conditions
869 using SPME, *J. Phys. Chem. A*, 109, 5358-5365, 10.1021/jp050166s, 2005.

870 Pan, X., Underwood, J. S., Xing, J. H., Mang, S. A., and Nizkorodov, S. A.:
871 Photodegradation of secondary organic aerosol generated from limonene oxidation by

872 ozone studied with chemical ionization mass spectrometry, *Atmos. Chem. Phys.*, 9, 3851-
873 3865, 10.5194/acp-9-3851-2009, 2009.

874 Park, J., Gomez, A. L., Walser, M. L., Lin, A., and Nizkorodov, S. A.: Ozonolysis and
875 photolysis of alkene-terminated self-assembled monolayers on quartz nanoparticles:
876 implications for photochemical aging of organic aerosol particles, *Physical Chemistry*
877 *Chemical Physics*, 8, 2506-2512, 10.1039/b602704k, 2006.

878 Paulot, F., Wunch, D., Crouse, J. D., Toon, G. C., Millet, D. B., DeCarlo, P. F.,
879 Vigouroux, C., Deutscher, N. M., Abad, G. G., Notholt, J., Warneke, T., Hannigan, J. W.,
880 Warneke, C., de Gouw, J. A., Dunlea, E. J., De Maziere, M., Griffith, D. W. T., Bernath,
881 P., Jimenez, J. L., and Wennberg, P. O.: Importance of secondary sources in the
882 atmospheric budgets of formic and acetic acids, *Atmos. Chem. Phys.*, 11, 1989-2013,
883 10.5194/acp-11-1989-2011, 2011.

884 Seco, R., Penuelas, J., and Filella, I.: Short-chain oxygenated VOCs: Emission and uptake
885 by plants and atmospheric sources, sinks, and concentrations, *Atmospheric Environment*,
886 41, 2477-2499, 10.1016/j.atmosenv.2006.11.029, 2007.

887 Sindelarova, K., Granier, C., Bouarar, I., Guenther, A., Tilmes, S., Stavrakou, T., Muller,
888 J. F., Kuhn, U., Stefani, P., and Knorr, W.: Global data set of biogenic VOC emissions
889 calculated by the MEGAN model over the last 30 years, *Atmos. Chem. Phys.*, 14, 9317-
890 9341, 10.5194/acp-14-9317-2014, 2014.

891 Singh, H., Chen, Y., Tabazadeh, A., Fukui, Y., Bey, I., Yantosca, R., Jacob, D., Arnold,
892 F., Wohlfrom, K., Atlas, E., Flocke, F., Blake, D., Blake, N., Heikes, B., Snow, J., Talbot,
893 R., Gregory, G., Sachse, G., Vay, S., and Kondo, Y.: Distribution and fate of selected
894 oxygenated organic species in the troposphere and lower stratosphere over the Atlantic,
895 *Journal of Geophysical Research-Atmospheres*, 105, 3795-3805, 10.1029/1999jd900779,
896 2000.

897 Slusher, D. L., Pitteri, S. J., Haman, B. J., Tanner, D. J., and Huey, L. G.: A chemical
898 ionization technique for measurement of pernitric acid in the upper troposphere and the
899 polar boundary layer, *Geophys. Res. Lett.*, 28, 3875-3878, 10.1029/2001gl013443, 2001.

900 Slusher, D. L., Huey, L. G., Tanner, D. J., Chen, G., Davis, D. D., Buhr, M., Nowak, J. B.,
901 Eisele, F. L., Kosciuch, E., Mauldin, R. L., Lefer, B. L., Shetter, R. E., and Dibb, J. E.:
902 Measurements of pernitric acid at the South Pole during ISCAT 2000, *Geophys. Res. Lett.*,
903 29, 10.1029/2002gl015703, 2002.

904 Sorooshian, A., Ng, N. L., Chan, A. W. H., Feingold, G., Flagan, R. C., and Seinfeld, J.
905 H.: Particulate organic acids and overall water-soluble aerosol composition measurements
906 from the 2006 Gulf of Mexico Atmospheric Composition and Climate Study (GoMACCS),
907 *Journal of Geophysical Research-Atmospheres*, 112, 16, 10.1029/2007jd008537, 2007.

908 Sorooshian, A., Murphy, S. M., Hersey, S., Bahreini, R., Jonsson, H., Flagan, R. C., and
909 Seinfeld, J. H.: Constraining the contribution of organic acids and AMS m/z 44 to the
910 organic aerosol budget: On the importance of meteorology, aerosol hygroscopicity, and
911 region, *Geophys. Res. Lett.*, 37, 5, 10.1029/2010gl044951, 2010.

912 Souza, S. R., and Carvalho, L. R. F.: Seasonality influence in the distribution of formic and
913 acetic acids in the urban atmosphere of Sao Paulo City, Brazil, *Journal of the Brazilian*
914 *Chemical Society*, 12, 755-762, 2001.

915 Spaulding, R. S., Talbot, R. W., and Charles, M. J.: Optimization of a mist chamber (cofer
916 scrubber) for sampling water-soluble organics in air, *Environmental Science &*
917 *Technology*, 36, 1798-1808, 10.1021/es011189x, 2002.

918 Talbot, R. W., Beecher, K. M., Harriss, R. C., and Cofer, W. R.: Atmospheric
919 Geochemistry of Formic and Acetic Acids at a Mid-latitude Temperate Site, *Journal of*
920 *Geophysical Research-Atmospheres*, 93, 1638-1652, 10.1029/JD093iD02p01638, 1988.

921 Talbot, R. W., Mosher, B. W., Heikes, B. G., Jacob, D. J., Munger, J. W., Daube, B. C.,
922 Keene, W. C., Maben, J. R., and Artz, R. S.: Carboxylic Acids in the Rural Continental
923 Atmosphere over the Eastern United States during the Shenandoah Cloud and
924 Photochemistry Experiment, *Journal of Geophysical Research-Atmospheres*, 100, 9335-
925 9343, 10.1029/95jd00507, 1995.

926 Talbot, R. W., Dibb, J. E., Scheuer, E. M., Blake, D. R., Blake, N. J., Gregory, G. L.,
927 Sachse, G. W., Bradshaw, J. D., Sandholm, S. T., and Singh, H. B.: Influence of biomass
928 combustion emissions on the distribution of acidic trace gases over the southern Pacific
929 basin during austral springtime, *Journal of Geophysical Research-Atmospheres*, 104, 5623-
930 5634, 10.1029/98jd00879, 1999.

931 Veres, P., Roberts, J. M., Warneke, C., Welsh-Bon, D., Zahniser, M., Herndon, S., Fall, R.,
932 and de Gouw, J.: Development of negative-ion proton-transfer chemical-ionization mass
933 spectrometry (NI-PT-CIMS) for the measurement of gas-phase organic acids in the
934 atmosphere, *Int. J. Mass Spectrom.*, 274, 48-55, 10.1016/j.ijms.2008.04.032, 2008.

935 Veres, P., Roberts, J. M., Burling, I. R., Warneke, C., de Gouw, J., and Yokelson, R. J.:
936 Measurements of gas-phase inorganic and organic acids from biomass fires by negative-
937 ion proton-transfer chemical-ionization mass spectrometry, *Journal of Geophysical*
938 *Research-Atmospheres*, 115, 10.1029/2010jd014033, 2010.

939 Veres, P. R., Roberts, J. M., Cochran, A. K., Gilman, J. B., Kuster, W. C., Holloway, J. S.,
940 Graus, M., Flynn, J., Lefter, B., Warneke, C., and de Gouw, J.: Evidence of rapid production
941 of organic acids in an urban air mass, *Geophys. Res. Lett.*, 38, 10.1029/2011gl048420,
942 2011.

943 Vlasenko, A., George, I. J., and Abbatt, J. P. D.: Formation of volatile organic compounds
944 in the heterogeneous oxidation of condensed-phase organic films by gas-phase OH, *J. Phys.*
945 *Chem. A*, 112, 1552-1560, 10.1021/jp0772979, 2008.

946 Walser, M. L., Park, J., Gomez, A. L., Russell, A. R., and Nizkorodov, S. A.:
947 Photochemical aging of secondary organic aerosol particles generated from the oxidation
948 of d-limonene, *J. Phys. Chem. A*, 111, 1907-1913, 10.1021/jp0662931, 2007.

949 Xu, L., Guo, H. Y., Weber, R. J., and Ng, N. L.: Chemical Characterization of Water-
950 Soluble Organic Aerosol in Contrasting Rural and Urban Environments in the Southeastern
951 United States, *Environmental Science & Technology*, 51, 78-88, 10.1021/acs.est.6b05002,
952 2017.

953 YataVELLI, R. L. N., Mohr, C., Stark, H., Day, D. A., Thompson, S. L., Lopez-Hilfiker, F.
954 D., Campuzano-Jost, P., Palm, B. B., Vogel, A. L., Hoffmann, T., Heikkinen, L., Aijala,
955 M., Ng, N. L., Kimmel, J. R., Canagaratna, M. R., Ehn, M., Junninen, H., Cubison, M. J.,
956 Petaja, T., Kulmala, M., Jayne, J. T., Worsnop, D. R., and Jimenez, J. L.: Estimating the
957 contribution of organic acids to northern hemispheric continental organic aerosol,
958 *Geophys. Res. Lett.*, 42, 6084-6090, 10.1002/2015gl064650, 2015.

959 Zhang, R. Y., Suh, I., Zhao, J., Zhang, D., Fortner, E. C., Tie, X. X., Molina, L. T., and
960 Molina, M. J.: Atmospheric new particle formation enhanced by organic acids, *Science*,
961 304, 1487-1490, 10.1126/science.1095139, 2004.

962

963

964

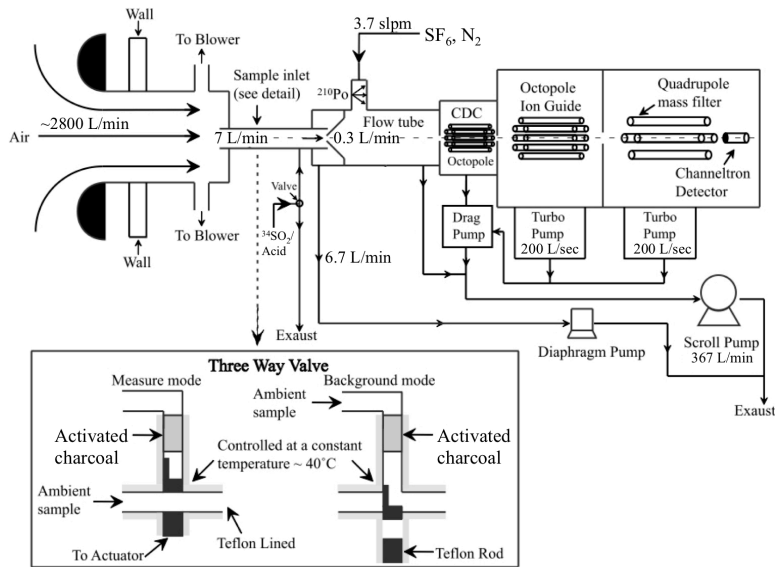
965

966

967

968

969



970

971 **Figure 1:** The CIMS instrument and inlet configuration used in the field study. The
 972 automated three-way sampling valve is shown in the inset. The figure was adapted from
 973 Liao et al. (2011).

974

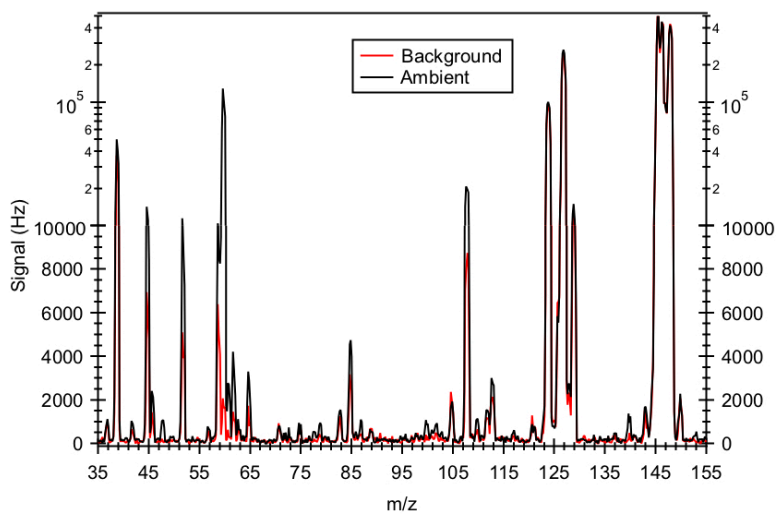
975

976

977

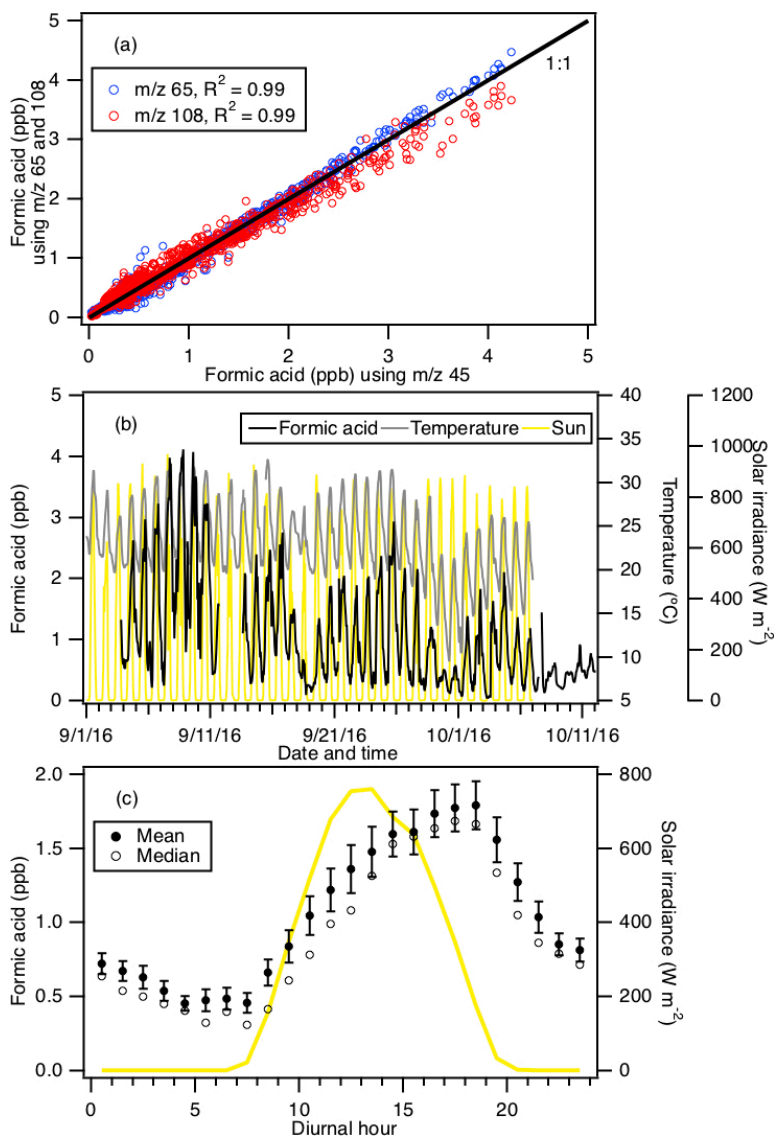
978

979



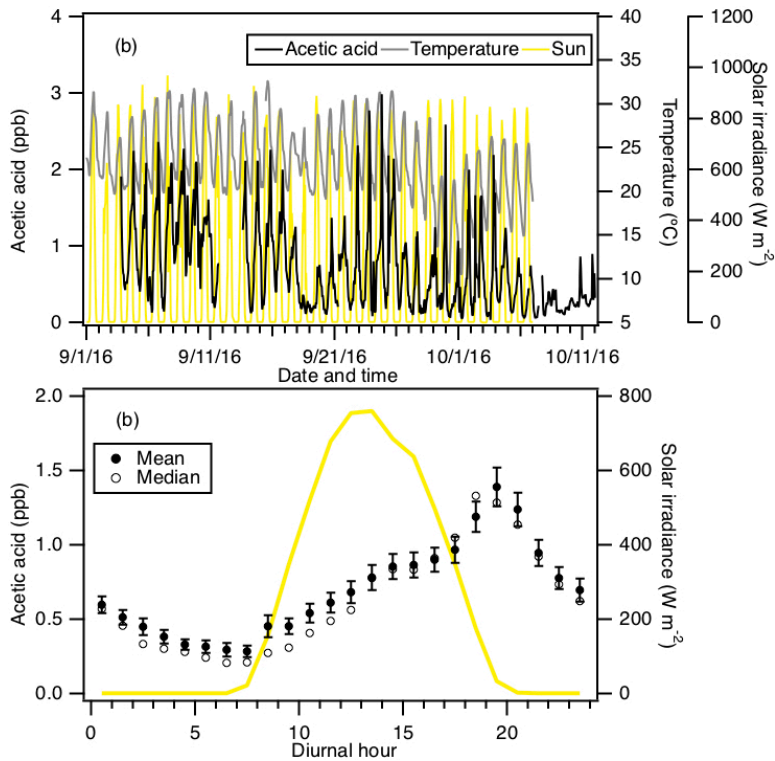
980

981 **Figure 2:** Mass spectrum of ambient air and background measured in Yorkville, Georgia
 982 on 8 Sept 2016 using SF₆⁻. Note that the ³²SF₆⁻ reagent ion signal (at m/z 146) is saturated,
 983 causing the sharp drop in its signal. As a result, the ion signal of its isotope ³⁴SF₆⁻ (at m/z
 984 150) was monitored to determine if the reaction of SF₆⁻ with ambient water vapor and O₃
 985 depleted SF₆⁻ reagent ions.



986

987 **Figure 3:** (a) Scatter plot comparison of ambient formic acid concentrations determined
 988 using mass peaks m/z 45, 65 and 108. The three datasets correlated well with one another
 989 ($R^2 = 0.99$). Linear regression of the data gave slopes of 1 (for m/z 65) and 0.95 (for m/z
 990 108), indicating that all three mass peaks can be used to determine the formic acid
 991 concentration. (b) Time series of formic acid concentration, temperature and solar
 992 irradiance. All the data are displayed as 1-hour averages. (c) Diurnal profiles of formic acid
 993 concentration (symbols) and solar irradiance (yellow line). All the concentrations represent
 994 averages in 1-hour intervals and the standard errors are plotted as error bars.



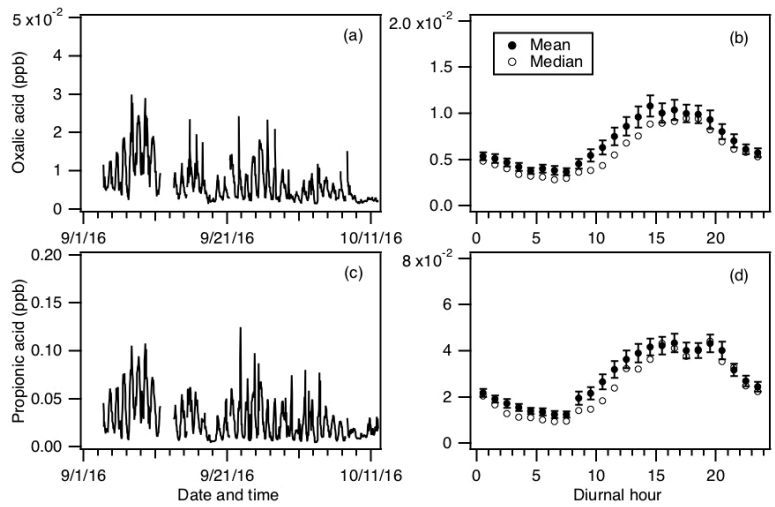
995

996 **Figure 4:** (a) Time series of acetic acid concentration, temperature and solar irradiance.
 997 All the data are displayed as 1-hour averages. (c) Diurnal profiles of acetic acid (symbols)
 998 and solar irradiance (yellow line). All the concentrations represent averages in 1-hour
 999 intervals and the standard errors are plotted as error bars.

1000

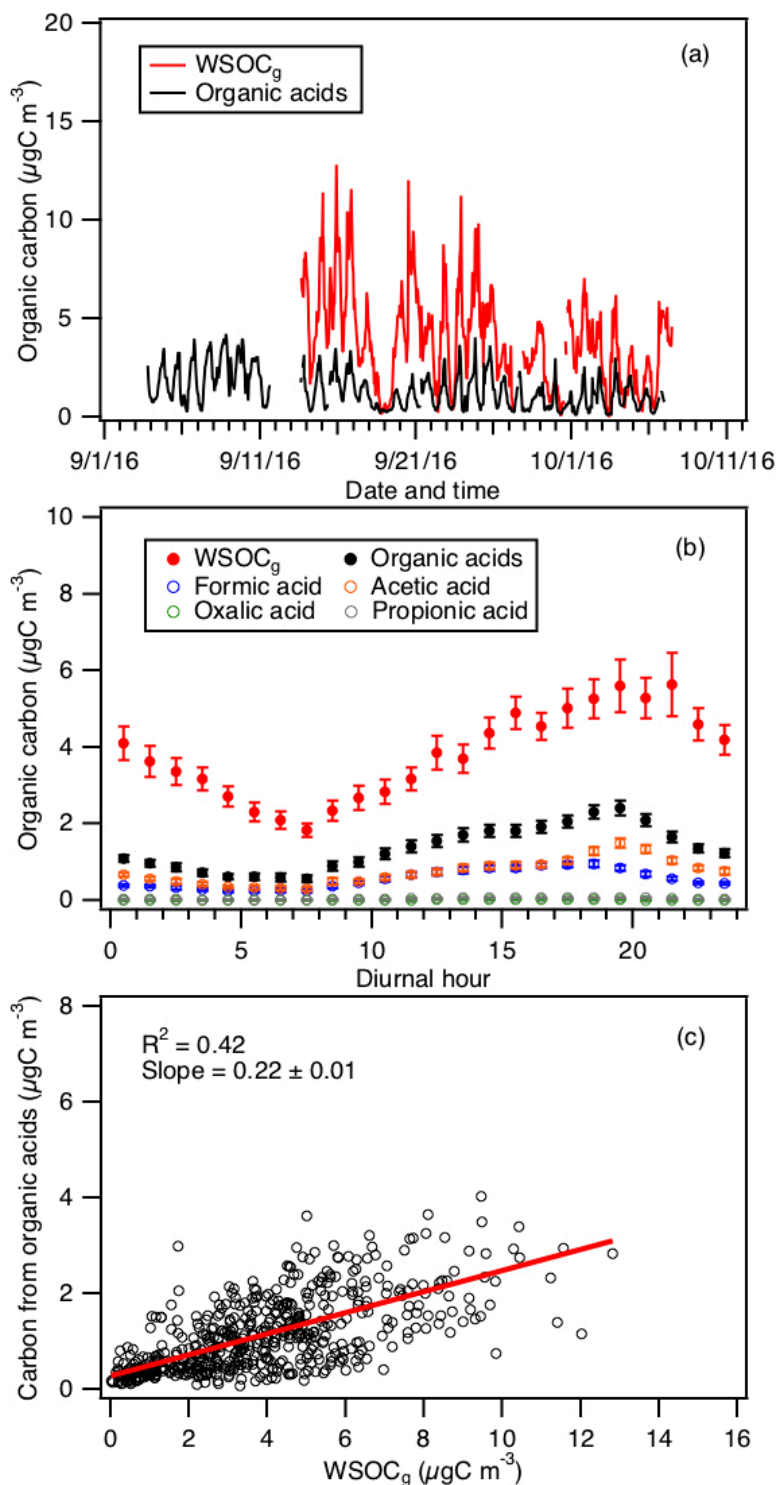
1001

1002



1003

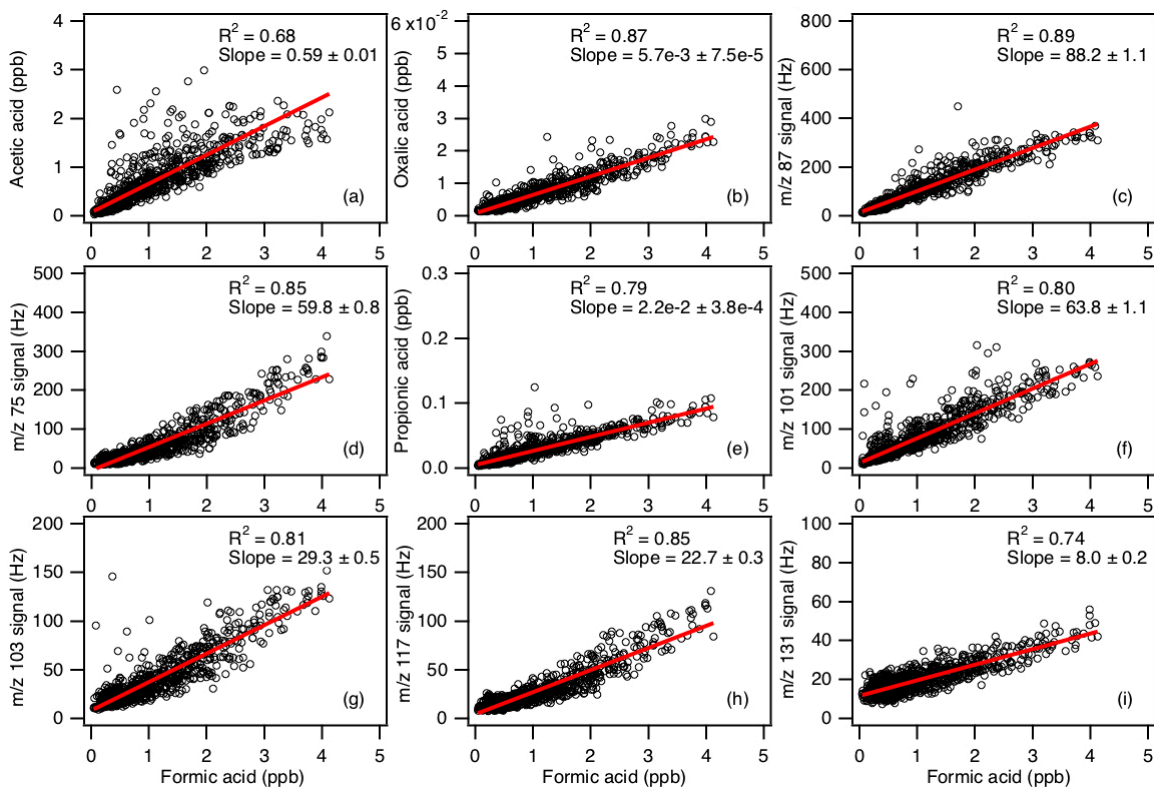
1004 **Figure 5:** Time series of concentrations of (a) oxalic and (c) propionic acids measured
 1005 during the field study. All the data are displayed as 1-hour averages. Their corresponding
 1006 diurnal profiles are shown in (b) and (d), respectively. The diurnal profile concentrations
 1007 represent averages in 1-hour intervals and the standard errors are plotted as error bars.



1008

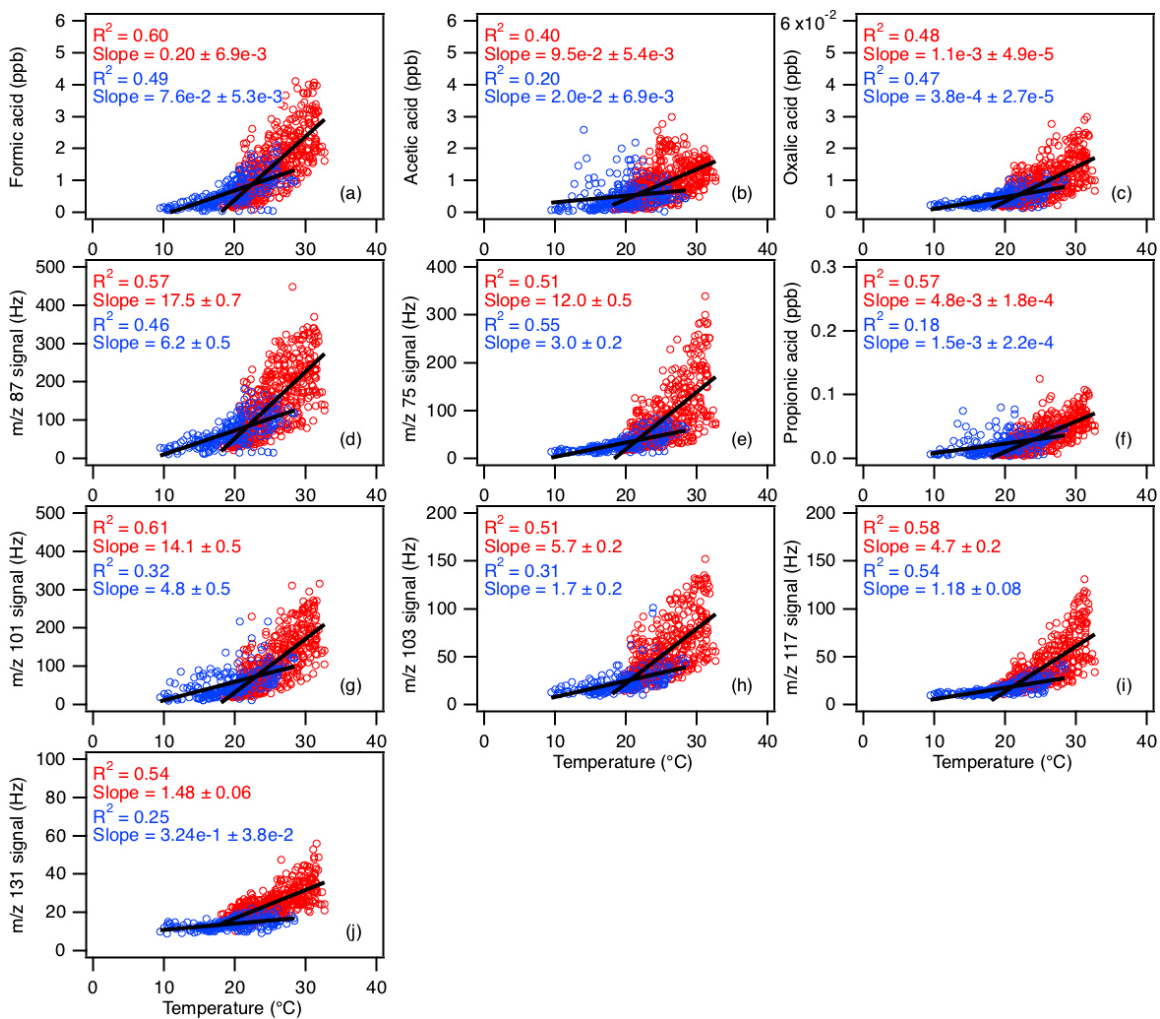
1009 **Figure 6:** (a) Time series of WSOC_g and the total organic carbon contributed by formic,
 1010 acetic, oxalic and propionic acids. All the data are displayed as 1-hour averages. (b) Diurnal
 1011 profiles of WSOC_g and the total organic carbon contributed by formic, acetic, oxalic and
 1012 propionic acids. Also shown are the diurnal profiles of the organic carbon contributed by

1013 the individual organic acids. All the concentrations represent the mean hourly averages and
1014 the standard errors are plotted as error bars. (c) Scatter plot of total organic carbon
1015 contributed by formic, acetic, oxalic and propionic acids with $WSOC_g$.



1016

1017 **Figure 7:** Scatter plots of concentrations (or ion signals) of the measured organic acids
1018 with formic acid concentration. All the data are displayed as 1-hour averages. Red lines
1019 shown are linear fits to the data.



1020

1021 **Figure 8:** Scatter plots of concentrations (or ion signals) of the measured organic acids
 1022 with ambient temperature. The red symbols are data collected from 3 to 27 Sept, while the
 1023 blue symbols are data collected from 28 Sept onwards. All the data are displayed as 1-hour
 1024 averages. Black lines shown are linear fits to the datasets.

1025

1026

1027

1028

1029

1030 **Table 1:** Summary of organic acids of interest, their detection limits and sensitivities of
 1031 their X⁻ and X⁻•HF ions^a

Organic Acid	Detection limit (ppt) ^b	Sensitivity (Hz ppt ⁻¹)	
		X ⁻	X ⁻ •HF
Formic acid	30	1.29 ± 0.22	0.29 ± 0.05
Acetic acid	60	1.46 ± 0.29	0.30 ± 0.06
Oxalic acid	1	6.38 ± 0.32	0.97 ± 0.05
Butyric acid	30	0.41 ± 0.01	0.12 ± 0.004
Glycolic acid	2	5.53 ± 0.11	1.64 ± 0.03
Propionic acid	6	2.05 ± 0.02	1.26 ± 0.01
Valeric acid	10	0.76 ± 0.008	0.35 ± 0.004

1032 ^aOnly organic acids with calibration measurements are shown.

1033 ^bDetection limits are approximated from 3 times the standard deviation values (3σ) of the
 1034 ion signals measured during background mode. Shown here are the average detection limits
 1035 of the organic acids for 2.5 min averaging periods which corresponds to the length of a
 1036 background measurement at a 4 % duty cycle for each mass.